Chapter 5B. Analysis of Imaging Spectrometer Data for the Daykundi Area of Interest

By Todd M. Hoefen, Daniel H. Knepper, Jr. and Stuart A. Giles

Abstract

Imaging spectrometer data collected over the Daykundi area of interest (AOI) in central Afghanistan were analyzed with spectroscopic methods to identify the occurrence of selected surficial material classes. Absorption features in the spectra of HyMap data were compared to a reference library of spectra of known materials. The HyMap data for the Daykundi AOI show good correlation to the various lithologic units of the region. The calcite, calcite + clays/micas, muscovite and illite classes cover most of the AOI. However, spatially contiguous patterns of dolomite, chlorite or epidote, montmorillonite, serpentine and kaolinite + muscovite/clay/calcite are mapped throughout the region. In the iron-bearing minerals map, the Fe^{2+} Fe^{3+} Type 2, goethite classes, Fe^{3+} Type 1, and Fe-hydroxide classes dominate the AOI, with smaller groupings of hematite and epidote occurring in several areas. The muscovite, illite, dolomite, serpentine, and Fe^{2+} Fe^{3+} Type 2 classes are all associated with different geologic units in the area. Most of the known mineral occurrences in the AOI are small or lack diagnostic spectral features, which makes them difficult to detect with the HyMap data. Therefore, very few of the unnamed, unknown or unclassified prospects can be correlated back to classes mapped with the HyMap sensor. For the larger prospects, the HyMap mapping results can usually be correlated back to the gangue minerals, deposit mineralogy or minerals associated with the host lithology.

5B.1 Introduction

Previous U.S. Geological Survey (USGS) analyses of existing geologic data of Afghanistan indicated areas with the potential for a variety of mineral resources (Peters and others, 2007). From these areas of interest, several were selected for follow-on studies using modern imaging spectrometer data to further characterize surface materials. Imaging spectroscopy is an advanced type of remote sensing also known as hyperspectral remote sensing. One such area is the Daykundi area of interest (AOI) in central Afghanistan.

The Daykundi area is approximately 200 kilometers (km) southwest of Kabul (fig. 5B–1), and is believed to have the potential for tin and tungsten deposits likely associated with Tertiary felsic intrusive rocks, as well as other potential resources (Peters and others, 2007). To help assess these potential resources, high resolution imaging spectrometer data were analyzed to detect the presence of selected minerals that may be indicative of past mineralization processes. This report contains the results of the imaging spectrometer data analyses and identifies numerous sites with the Daykundi area that deserve further investigation, especially detailed geological mapping and geochemical studies.

5B.2 Data Collection and Processing

In 2007, imaging spectrometer data were acquired over most of Afghanistan as part of the USGS Oil and Gas Resources Assessment of the Katawaz and Helmand Basins project. These data were collected to characterize surface materials in support of assessments of resources (coal, water, minerals, oil, and gas) and earthquake hazards in the country (King and others, 2010). Imaging spectrometers measure the reflectance of visible and near-infrared light from the Earth's surface in many narrow channels, producing a reflectance spectrum for each image pixel. These reflectance spectra can be interpreted to identify absorption features that arise from specific chemical transitions and molecular

bonds that provide compositional information about surface materials. Imaging spectrometer data can only be used to characterize the surface materials and not subsurface composition or structure. However, subsurface processes can be indicated by the distribution of surface materials that can be detected using imaging spectroscopy data.

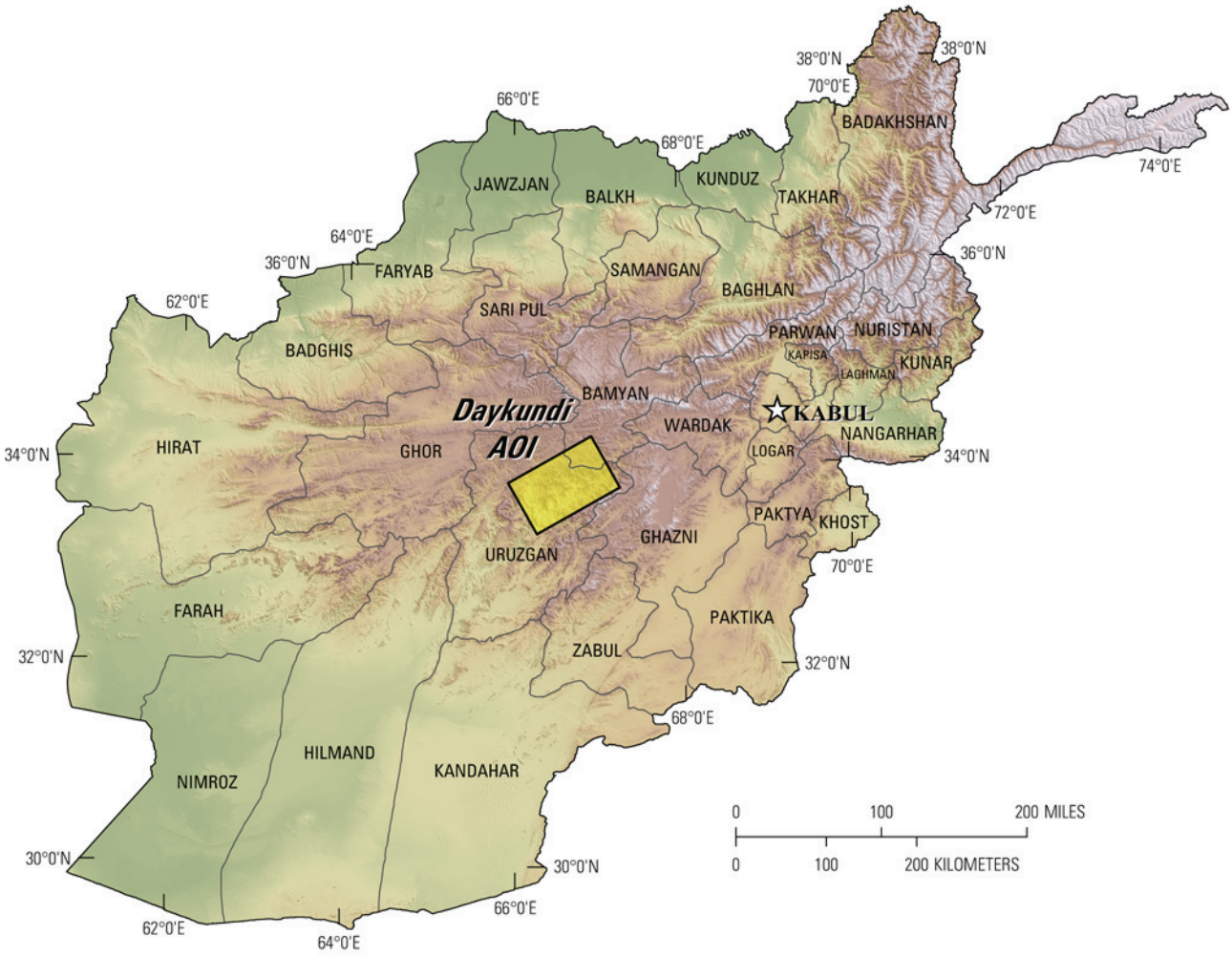

Figure 5B–1. Index map of the Daykundi area of interest, northeastern Afghanistan.

5B.2.1 Collection of Imaging Spectrometer Data

The HyMap imaging spectrometer (Cocks and others, 1998) was flown over Afghanistan from August 22 to October 2, 2007 (Kokaly and others, 2008). HyMap has 512 cross-track pixels and covers the wavelength range from 0.43 to 2.48 microns (µm) in 128 channels. The imaging spectrometer was flown on a WB-57 high-altitude aircraft at 50,000 feet. There were 207 standard data flight lines and 11 cross-cutting calibration lines collected over Afghanistan for a total of 218 flight lines, covering a surface area of 438,012 square kilometers (km^2) (Kokaly and others, 2008). Data were received in scaled radiance form (calibrated to National Institute of Standards and Technology reference materials). Before processing, four channels that had low signal-to-noise ratios and (or) were in wavelength regions overlapped by adjacent detectors were removed from the image cubes. Each flight line was georeferenced to Landsat base imagery in Universal Transverse Mercator (UTM) projection (Davis, 2007).

5B.2.2 Calibration Process

HyMap data were converted from radiance to reflectance using a multi-step calibration process. This process removed the influence of the solar irradiance function, atmospheric absorptions and residual instrument artifacts, resulting in reflectance spectra that have spectral features that arise from the material composition of the surface. Because of the extreme topographic relief and restricted access to ground calibration sites, modifications to the standard USGS calibration procedures were required to calibrate the 2007 Afghanistan HyMap dataset (Hoefen and others, 2010). In the first step of the calibration process, the radiance data were converted to apparent surface reflectance using the radiative transfer correction program Atmospheric CORrection Now (ACORN; ImSpec LLC, Palmdale, Calif.). ACORN was run multiple times for each flight line, using average elevations in 100-meter (m) increments, covering the range of minimum to maximum elevation within the flight line. A single atmospherically corrected image was assembled from these elevation-incremented ACORN results. This was done by determining the elevation of each HyMap pixel and selecting the atmospherically corrected pixel from the 100-m increment closest to that elevation.

Each assembled atmospherically corrected image was further empirically adjusted using ground-based reflectance measurements from a ground calibration site. Five ground-calibration spectra were collected in Afghanistan: Kandahar Air Field, Bagram Air Base, and Mazar-e-Sharif Airport, as well as soil samples from two fallow fields in Kabul. At each site, the average field spectrum of the ground target was used to calculate an empirical correction factor using the pixels of atmospherically corrected HyMap data in the flight lines that passed over the site. Subsequently, each of the HyMap flight lines was ground-calibrated using the empirical correction from the closest calibration site.

To further improve the data quality, an additional calibration step was taken to address the atmospheric differences caused, in part, by the large distances between the calibration sites and the survey areas. The large distances were a result of the lack of safe access to ground calibration sites. The duration of the airborne survey and variation in time of day during which flight lines were acquired also resulted in differences in atmospheric conditions between standard flight lines and lines over ground calibration sites, which were used to derive the empirical correction factors. Over the course of data collection, the sun angle, atmospheric water vapor, and atmospheric scattering differed for each flight line. To compensate for this variation, cross-cutting calibration flight lines over the ground calibration areas were acquired (Kokaly and others, 2008) and used to refine the reflectance calculation for standard data lines. A multiplier correction for standard data lines, typically oriented as north-south flight lines, was derived using the pixels that overlapped the well-calibrated cross-cutting lines, subject to slope, vegetation cover, and other restrictions on pixel selection (Hoefen and others, 2010). As a result, the localized cross-calibration multiplier, derived from the overlap region, reduced residual atmospheric contamination in the imaging spectrometer data that may have been present after the ground calibration step.

5B.2.3 Materials Maps and Presentation

After undergoing the above calibration process, the georeferenced and calibrated reflectance data were processed. The reflectance spectrum of each pixel of HyMap data was compared to the spectral features of reference entries in a spectral library of minerals, vegetation, water, and other materials (King, Kokaly, and others, 2011; Kokaly and others, 2011). The best spectral matches were determined for each pixel and the results were clustered into classes of materials discussed next.

HyMap reflectance data were processed using MICA (Material Identification and Characterization Algorithm), a module of the USGS Processing Routines in IDL (Interactive Data Language) for Spectroscopic Measurements (PRISM) software (Kokaly, 2011). The MICA analysis compared the reflectance spectrum of each pixel of HyMap data to entries in a reference spectral library of minerals, vegetation, water, and other materials. The HyMap data were compared to 97 reference spectra of well-characterized mineral and material standards. The resulting maps of material distribution,

resampled to 23 × 23 m square pixel grid, were mosaicked to create thematic maps of surface mineral occurrences over the full dataset covering Afghanistan.

The MICA module was applied to HyMap data twice to present the distribution of two categories of minerals that are naturally separated in the wavelength regions of their primary absorption features. MICA was applied using the subset of minerals with absorption features in the visible and near-infrared wavelength region, producing a 1-µm map of iron-bearing minerals and other materials (King, Kokaly, and others, 2011), and again using the subset of minerals with absorption features in the shortwave infrared, producing a 2-µm map of carbonates, phyllosilicates, sulfates, altered minerals, and other materials. For clarity of presentation, some individual classes in these two maps were bundled by combining selected mineral types (for example, all montmorillonites or all kaolinites) and representing them with the same color in order to reduce the number of mineral classes. The iron-bearing minerals map has 28 classes. Iron-bearing minerals with different mineral compositions but similar broad spectral features are difficult to classify as specific mineral species. Thus, generic spectral classes, including several minerals with similar absorption features, such as Fe^{3+} Type 1 and Fe^{3+} Type 2, are depicted on the map. The carbonates, phyllosilicates, sulfates, and altered minerals map has 32 classes. Minerals with slightly different compositions but similar spectral features are less easily discriminated, thus, some identified classes consist of several minerals with similar spectra, such as the "chlorite or epidote" class. When comparisons with reference spectra provided no viable match, a designation of "not classified" was assigned to a pixel.

5B.3 Geologic Setting of the Daykundi Area of Interest

The Daykundi AOI is within the Uruzgan and Bamyan provinces in central Afghanistan, and covers approximately 6,838 km^2. The contrast-enhanced stretch of the natural-color composite of Landsat Thematic Mapper (TM) bands in figure 5B–2 provides a general overview of the Daykundi AOI terrain, and is useful for understanding the general characteristics and distribution of surficial material, including rocks and soil, unconsolidated sediments, vegetation, and hydrologic features.

5B.3.1 Topography

Elevations in the Daykundi AOI range from 1,317 to 4,267 m (fig. 5B–3), the lowest of which are in the southern and southwestern regions. The highest elevations are in the central and eastern sections of the AOI. There are three district population centers within the AOI: Waras in the northeast, Khisraw in the central region, and Gizab in the southwest.

5B.3.2 Lithology and Structure

Rocks in the Daykundi AOI range in age from Proterozoic to Late Quaternary and Recent (fig. 5B–4; Doebrich and others, 2006; Abdullah and Chymriov, 1977). The stratified rocks range in age from Proterozoic to Late Quaternary and Recent, with a majority of the rocks in the southern two-thirds of the AOI being Late Proterozoic in age. Rocks along the northern edge of the AOI are mainly Middle Proterozoic in age. The southern and southwestern regions have extensive areas of Paleozoic and Mesozoic age rocks that are commonly bounded by faults. Cenozoic rocks occur in small units throughout the AOI, with one larger unit of Late Quaternary and Recent stratified rock units occurring in the southwestern corner (Doebrich and others, 2006; Abdullah and Chymriov, 1977; Peters and others, 2007).

Intrusive rocks within the Daykundi AOI range in age from Proterozoic to Late Cretaceous-Paleocene. The largest intrusive bodies are granitic and granodioritic Oligocene-age rocks that occur in the southern half of the AOI. These granitic/granodioritic rocks are expressed in the TM data as a light white-colored unit (see fig. 5B–2). A large mass of Miocene nepheline syenite intrudes the Proterozoic stratified rocks in the southeastern corner (Peters and others, 2007).

The Daykundi AOI includes the Oruzgan ore district and the Taghawlor pegmatite field. The Taghawlor lithium pegmatite field (lat 33°42'30" to 33°47'00" N, long 66°19'30" to 66°29'00" E) is

located in the west-central region of the AOI. The Taghawlor pegmatite field is a linearly elongated, nearly east-west-trending zone of steeply dipping tabular pegmatite veins with common spodumene (Peters and others, 2007). The pegmatite veins forming the field are within the contact zone of a pluton composed of biotite granodiorite and granite of the Helmand Complex, primarily in contact with Upper Proterozoic quartz-chlorite and quartz-chlorite-biotite schists. More than 200 steeply-dipping spodumene pegmatite veins concordant with the country rocks are known within the field. The veins vary from 100 to 1,500-m long and from 1 to 20-m wide (Peters and others, 2007). The large field of spodumene pegmatites discovered in the Helmand zone and the wide distribution of pegmatites and granites in the Helmand complex both indicate that the Helmand-Argandab Uplift is a promising source of rare metals (Peters and others, 2007).

The principal metals in the Oruzgan District are tungsten and tin present in skarn-scheelite, quartz-wolframite and quartz-scheelite rock units. The subordinate metals are copper, lead and zinc, occurring in a quartz-sulfide, skarn pyrite-chalcopyrite and magnetite-chalcopyrite rock units (Peters and others, 2007). Mineralized skarns were formed at the contacts between Oligocene granites and Devonian limestones (Peters and others, 2007).

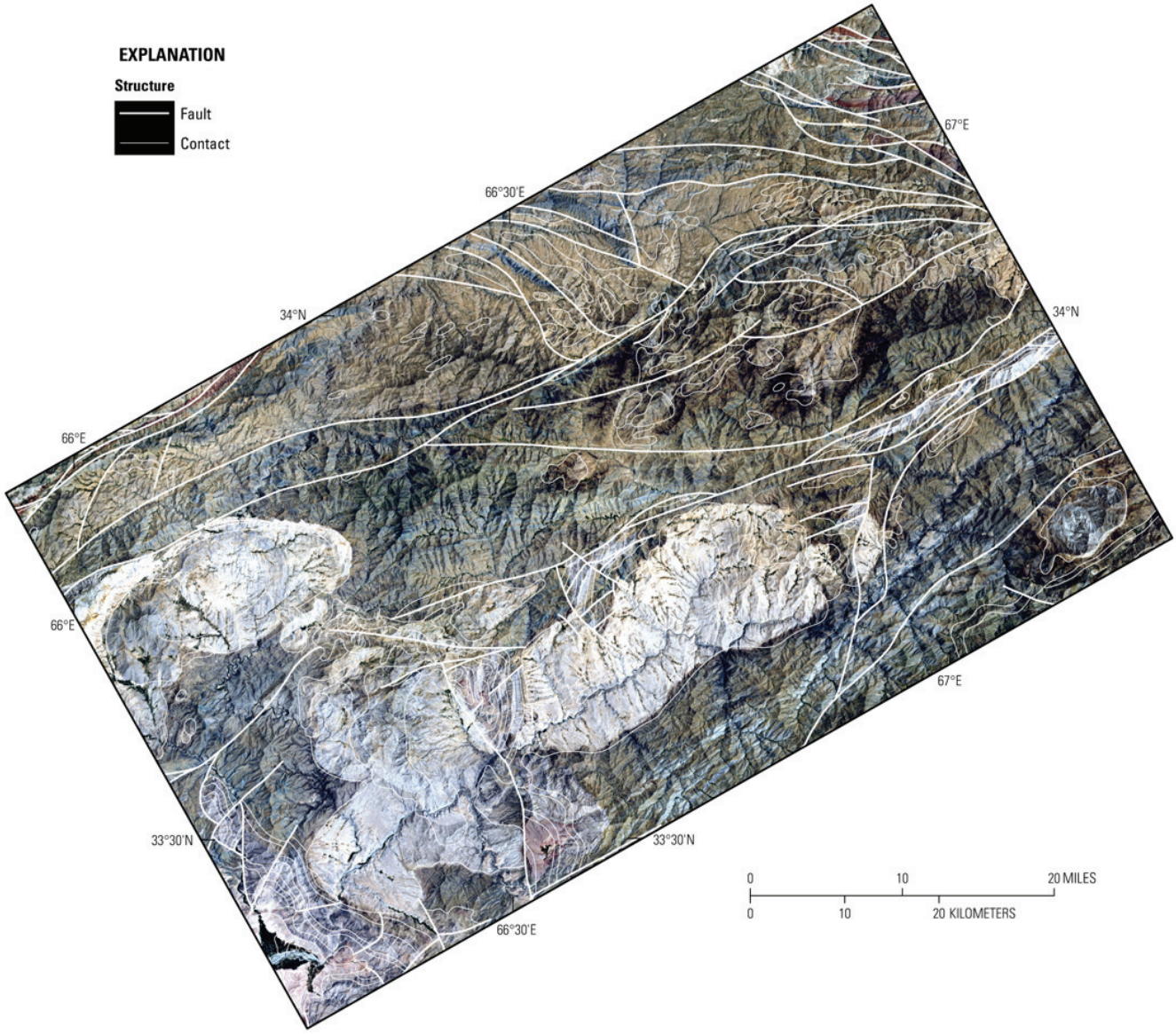

Figure 5B–2. Contrast-enhanced Landsat Thematic Mapper natural-color image of the Daykundi area of interest. Geologic contacts and faults from Doebrich and others (2006) and Abdullah and Chmyriov (1977).

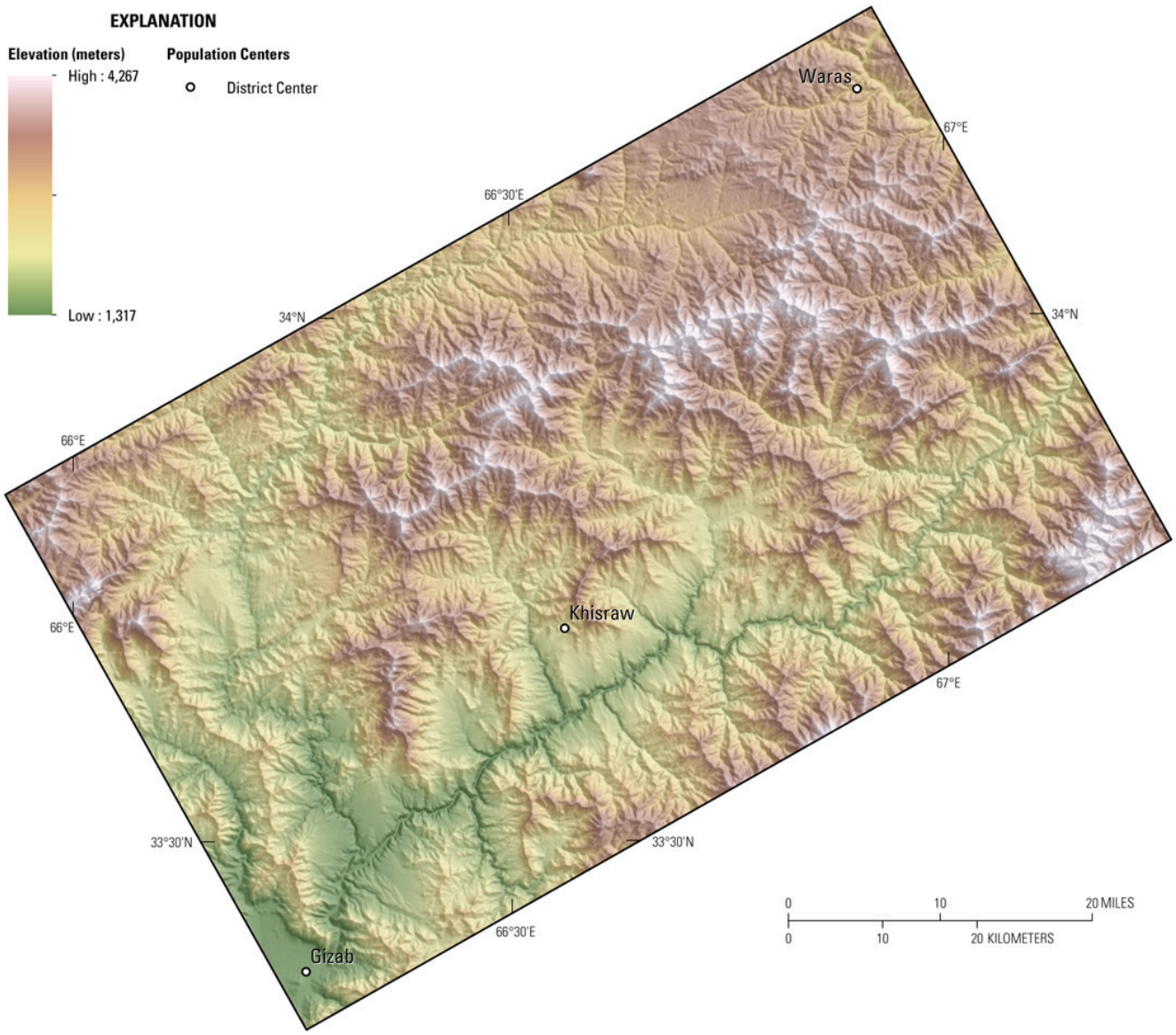

Figure 5B–3. Elevations and topography of the Daykundi area of interest.

5B.3.3 Known Mineralization

Figure 5B–5 shows 49 locations where mineralization with a potential for resource development may exist within the Daykundi AOI (Doebrich and others, 2006; Peters and others, 2007; Abdullah and others, 1977). The characteristics of the mineralized locations are summarized in table 5B–1, including a number of unnamed tin, tungsten, and polymetallic prospects. The named mineral occurrences are discussed in more detail in this section of the report. Table 5B–2 includes only the named mineral occurrences and adds additional information about the HyMap classifications associated with each one.

The Taghawlor deposit (lat 33°46'07"N, long 66°24'58"E) is located in the west-central region of the AOI. The deposit extends for 500 to 1,800 m, ranging in thickness from 2 to 20 m. The deposit occurs in pegmatites among Proterozoic shales in the exocontact zone of Oligocene granites (Doebrich and others, 2006; Abdullah and Chymriov, 1977; Peters and others, 2007). The Kunak pegmatite deposit (lat 34°00'00" N, long 66°41'23" E) is located in the north-northwestern region of the AOI. The deposit occurs in pegmatites located among Proterozoic shales and gneisses that are 1.5 to 20 m thick and extend from ten to hundreds of meters.

A number of unnamed tin, tungsten and polymetallic prospects are present in the Daykundi AOI (Peters and others, 2007; Abdullah and others, 1977: Doebrich and others, 2006). These unnamed

prospects are usually very small showings of the prospect and are not discussed herein. The Sheng prospect is a tin prospect located near lat 33°44'39"N, long 66°39'45"E. The area of the occurrence includes about 300 quartz veins and silicified zones in an intrusion of Oligocene granite. The veins vary between 1 and 15 centimeters (cm) in thickness, amounting to 1 m in swells, and between 10 and 100 m in length. The zones range from 0.3 to 1.5 m in width and from 30 to 100 m in length. The mineral composition of veins is as follows: quartz, pyrite, chalcopyrite, arsenopyrite, galena, limonite, malachite, and azurite, scarcely disseminated cassiterite, and scheelite grains (Peters and others, 2007; Abdullah and others, 1977; Doebrich and others, 2006).

The Eskan polymetallic prospect is located near lat 33°45'00"N, long 66°47'00"E, in a 25-m-wide and 300-m-long fault zone within Oligocene granite. The prospect is ochre colored and impregnated by quartz stringers (Abdullah and others, 1977; Doebrich and others, 2006).

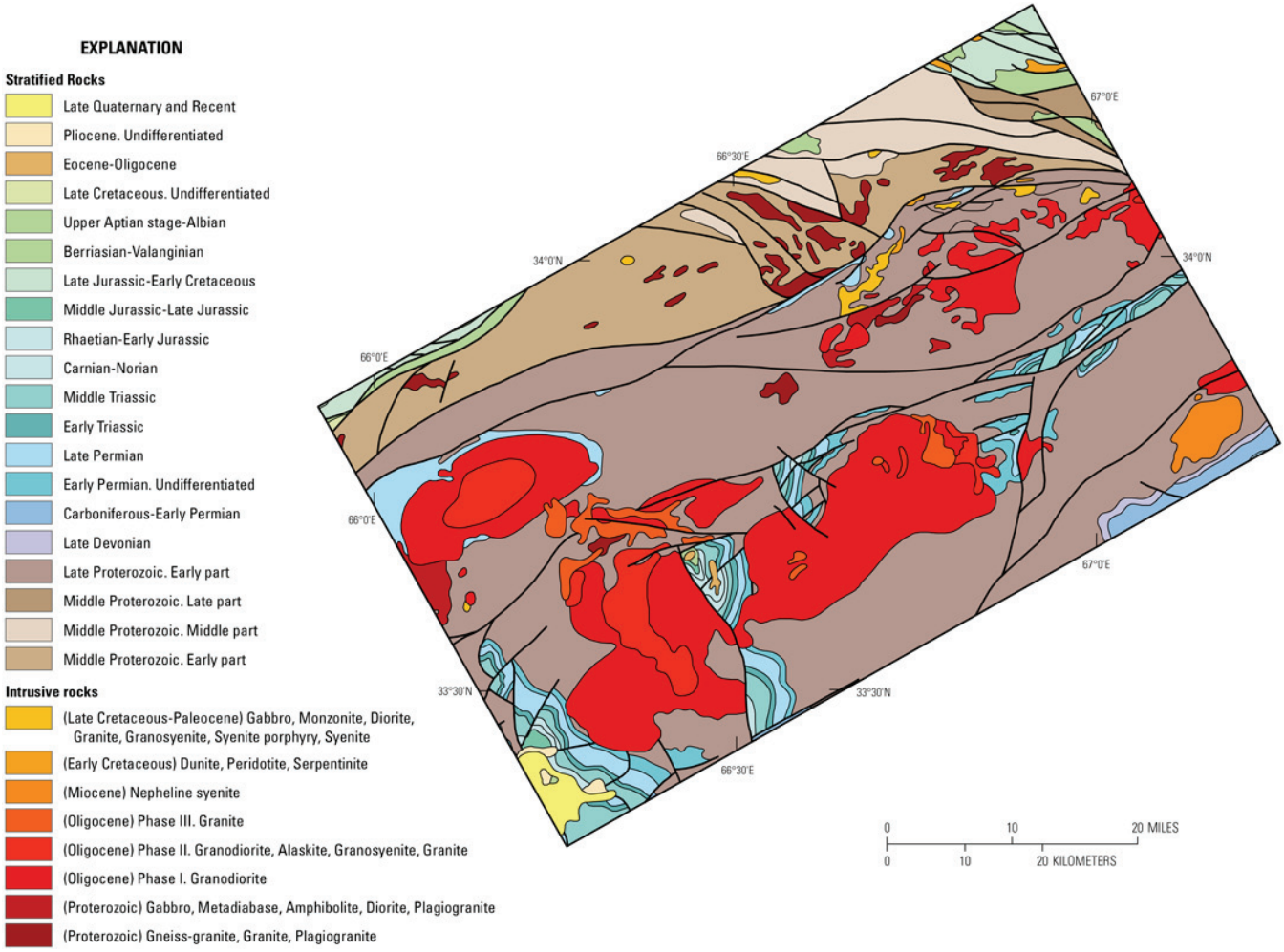

Figure 5B–4. Geologic map of the Daykundi area of interest from 1:500,000-scale geologic map of Afghanistan (Doebrich and others, 2006; Abdullah and Chmyriov, 1977).

The Daykundi AOI has several known tungsten prospects. The Charkh tungsten prospect is located in the central region of the AOI near lat 33°54'10"N, long 66°38'00"E. The prospect contains a zone of shattered and ochreous rock, 1 to 2 m in width and more than 100 m in length, and is outlined in Oligocene granite and Proterozoic schist (Peters and others, 2007; Abdullah and others, 1977; Doebrich and others, 2006). The Salej prospect is in the northwestern region (lat 33°51'30"N, long 66°20'30"E) of the AOI. Proterozoic rock inliers have been found in a stock 400 × 1,500 m in size, of altered granodiorite of Oligocene age (Peters and others, 2007; Abdullah and others, 1977; Doebrich and others, 2006). The Nili prospect occurs between lat 33°43'20"N - 33°46'00"N, long 66°07'00"E - 66°12'30"E.

Oligocene granite encloses several scheelite-bearing zones of greisens, 18 km2 in area, consisting of silicified and muscovitized rocks with scarcely disseminated scheelite, wolframite, and copper sulfides (Peters and others, 2007; Abdullah and others, 1977; Doebrich and others, 2006). The Chak prospect is located at lat 33°41'40"N, long 66°10'40"E. Two skarn lenses (one 0.1–0.2 to 10 m thick × 150 m long, the other 45 m thick × 65 m long) have been found in the contact zone between an intrusion of Oligocene granite and Permian marble, forming a roof remnant (Peters and others, 2007; Abdullah and others, 1977; Doebrich and others, 2006). The Dariw-Sheng prospect (lat 33°45'17"N, long 66°44'51"E) located in the south-central region of the AOI occurs in Oligocene granites in shattered mineralized zones with thicknesses of up to 30 m and extending for a few hundred meters (Doebrich and others, 2006; Abdullah and others, 1977; Peters and others, 2007). The Charh II prospect is located near lat 33°54'11"N, long 66°38'00"E in Oligocene age granodiorites/granites (Abdullah and others, 1977; Doebrich and others, 2006).

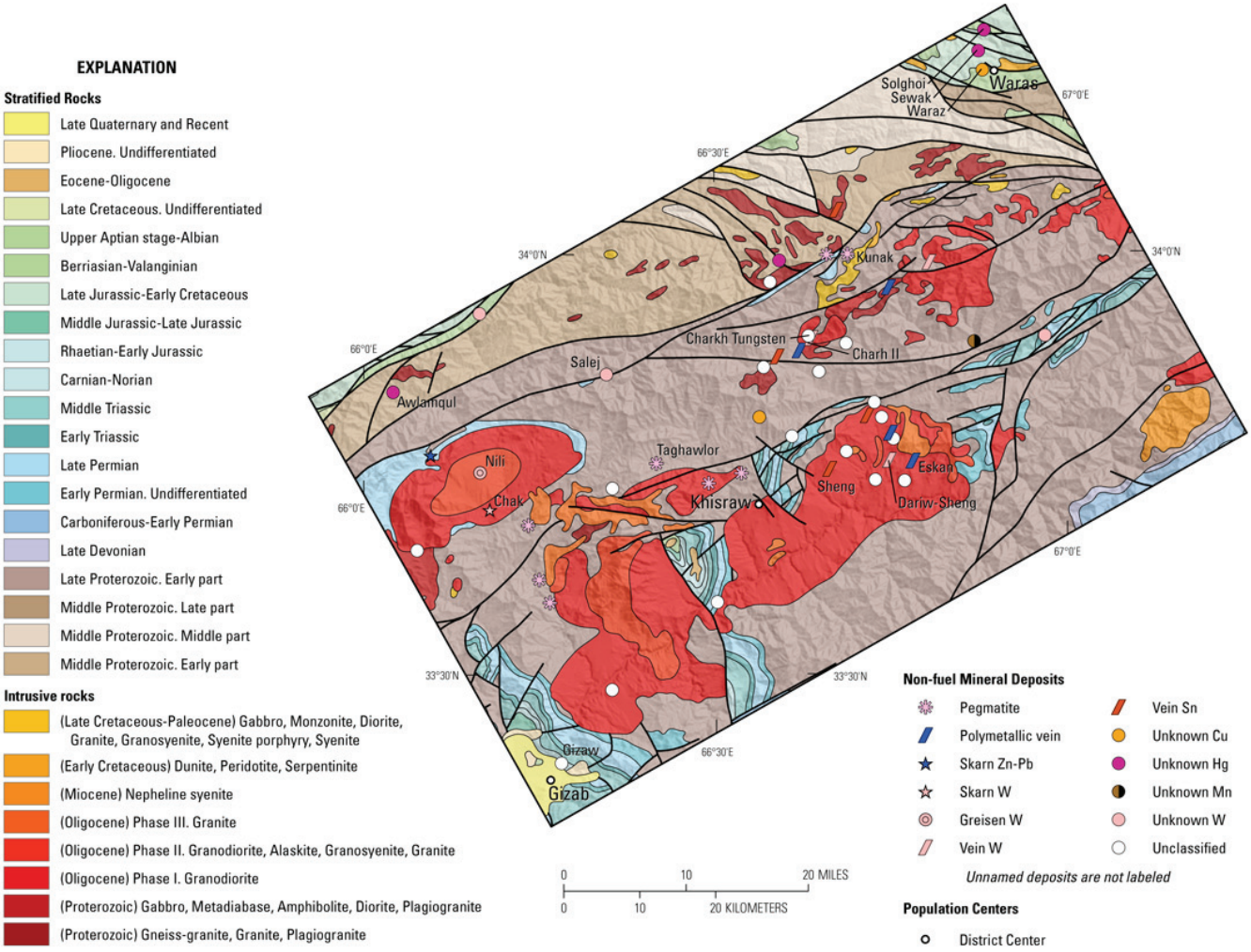

Figure 5B–5. Sites of known mineralization by deposit type (Peters and others, 2007; Doebrich and others, 2006; Abdullah and others, 1977) on the geologic map of the Daykundi area of interest from 1:500,000-scale geologic map of Afghanistan (Doebrich and others, 2006; Abdullah and Chmyriov, 1977).

Table 5B–1. Sites of known mineralization in the Daykundi area of interest (Doebrich and others, 2006; Abdullah and others, 1977; Peters and others, 2007).

[Cu, copper; Hg, mercury; K, potassium; Mn, manganese; Sn, tin; W, tungsten; Unk, unknown]

Name	Deposit type	Host	Alteration	Mineralogy	Gangue
Kunak	Pegmatite	Pegmatites among Proterozoic shales and gneisses	No data	Muscovite; garnet; cassiterite; orthite	Quartz; oligoclase
Taghawlor deposit	Pegmatite	Pegmatites among Proterozoic shales in exocontact zone of Oligocene granites massif	Albitization	Spodumene; columbite-tantalite; cassiterite	Albite; microcline
Unnamed	Pegmatite	Pegmatites among Proterozoic metamorphic rocks	No data	No data	No data
Unnamed	Pegmatite	Pegmatites among Proterozoic metamorphic rocks	No data	No data	No data
Unnamed	Pegmatite	Pegmatites among Proterozoic metamorphic rocks	No data	No data	No data
Unnamed	Pegmatite	Pegmatites among Oligocene granitoids	No data	Sulfides	No data
Unnamed	Pegmatite	Pegmatites among Proterozoic metamorphic rocks	No data	No data	No data
Unnamed	Pegmatite	Proterozoic pegmatites	Silicification; tourmalinization	Cassiterite	Quartz; microcline; muscovite; tourmaline
Eskan	Polymetallic vein	Oligocene granites	Silicification; limonitization	Limonite	Quartz
Unnamed	Polymetallic vein	Oligocene granites	Silicification	Fahlore	Quartz
Unnamed	Polymetallic vein	Proterozoic silty sandstones	Silicification; hornfels	Sulfides	Quartz
Unnamed	Polymetallic vein	Proterozoic diorites and plagiogranites	Quartz-tourmaline alteration	Sulfides	Quartz; tourmaline
Unnamed	Skarn zn-pb	Proterozoic marbled limestones	Skarn alteration	Sulfides	No data
Gizaw	Unclassified	Upper Triassic limestones	Calcite alteration	Iceland spar	No data
Unnamed	Unclassified	Carboniferous - Permian limestones forming an Oligocene granitoids massif remnant	Silicification	No data	Quartz
Unnamed	Unclassified	Oligocene granites	No data	Malachite	No data
Unnamed	Unclassified	Oligocene granites	No data	Malachite	No data
Unnamed	Unclassified	Pegmatites among Proterozoic metamorphic rocks	No data	No data	Muscovite; tourmaline
Unnamed	Unclassified	Oligocene granites	K-feldspar alteration; quartz alteration	Pyrite	Quartz
Unnamed	Unclassified	Oligocene granites	Quartz alteration; limonitization	Sulfides; limonite; malachite	Quartz
Unnamed	Unclassified	Oligocene granites	Silicification	Sulfides	Quartz
Unnamed	Unclassified	Oligocene granites	Silicification; limonitization	Limonite	Quartz
Unnamed	Unclassified	Oligocene pegmatites and granites in Proterozoic metamorphosed rocks	No data	Sulfides	No data
Unnamed	Unclassified	Oligocene granites	No data	No data	No data

Name	Deposit type	Host	Alteration	Mineralogy	Gangue
Unnamed	Unclassified	Proterozoic schists in contact with Oligocene granitoids massif	Hornfels	No data	No data
Unnamed	Unclassified	Proterozoic cherty rocks	Silicification; limonitization	Limonite; malachite	Quartz
Unnamed	Unclassified	Proterozoic granito-gneisses	No data	No data	No data
Unnamed	Unclassified	Proterozoic schists	No data	Malachite	No data
Unnamed	Unclassified	Proterozoic granito-gneisses	Limonitization; chloritization	Limonite	Chlorite
Unnamed	Unk cu	A lamprophire dike in oligocene granites	No data	Sulfides	No data
Waraz	Unk cu	In the fracture zone which separates lower cretaceous ultrabasites from terrigenous-carbonate deposits of the same age	Carbonatization	Malachite; azurite	No data
Awlamqul	Unk hg	Lower cretaceous limestones	Recrystallization; calcite alteration	Cinnabar; pyrite; hematite; realgar	Calcite; siderite; ankerite
Sewak	Unk hg	Upper jurassic - lower cretaceous limestones	Hematitization	Cinnabar; hematite	No data
Solghoi	Unk hg	Lower cretaceous pebble conglomerates	Recrystallization; bleaching; silicification; dickitization	Cinnabar; metacinnabarite; pyrite; hematite; chalcopyrite	Quartz; dickite; calcite; siderite; ankerite; barite
Unnamed	Unk hg	Proterozoic metamorphic rocks	Carbonatization; dickitization; limonitization	Cinnabar	Limonite; carbonate
Unnamed	Unk mn	Cherty-marl rocks among the proterozoic formations	No data	No data	No data
Sheng	Vein sn	Oligocene granites	Quartz alteration; silicification; limonitization	Pyrite; chalcopyrite; arsenopyrite; galena; limonite; malachite; azurite; cassiterite; scheelite	Quartz; muscovite; chlorite
Unnamed	Vein sn	Oligocene granites	Quartz alteration; silicification	Cassiterite; sulfides	Quartz
Unnamed	Vein sn	Proterozoic rocks in contact with oligocene granites	Silicification	Cassiterite	Quartz
Unnamed	Vein sn	No data	Quartz-tourmaline alteration	Cassiterite	Quartz; tourmaline
Chak	W skarn	A contact of Oligocene granites and Permian marbles forming a roof remnant	Skarn alteration	Scheelite	No data
Charkh Tungsten	W unclassified	Oligocene granites and Proterozoic schists	Limonitization	No data	No data
Salej	W unknown	Xenoliths of Proterozoic rocks within Oligocene granitoids stock	No data	No data	No data
Unnamed	W unknown	Lower Triassic limestones	No data	No data	No data
Unnamed	W unknown	Lower Cretaceous red sandstones	No data	Sulfides	No data
Charh II	W vein	No data	No data	No data	No data
Dariw-Sheng	W vein	Oligocene granites	Silicification; Quartz alteration	Pyrite; chalcopyrite; fahlore; cassiterite; scheelite; malachite;	Quartz

Name	Deposit type	Host	Alteration	Mineralogy	Gangue
Nili	W vein	Oligocene granites	Greisen alteration; Quartz alteration	Scheelite; wolframite; pyrite; chalcopyrite; bornite; cassiterite; bismuthinite; arsenopyrite	Quartz; muscovite
Unnamed	W vein	Proterozoic metamorphic rocks in contact with Oligocene granitoids	Quartz alteration	Wolframite; quartz	Quartz

Table 5B–2. Larger sites of known mineralization in the Daykundi area of interest that have names (Doebrich and others, 2006; Abdullah and others, 1977; Peters and others, 2007).

[HyMap classifications are included for the 1- and 2-µm maps as they relate to the immediate area around the known mineral resource. An additional column for each classification lists nearby mineral groups that could be associated with each known mineral occurrence. Cu, copper; Hg, mercury; W, tungsten; Unk, unknown]

Name	Deposit type	Host lithology	Alteration	Mineralogy	Gangue	HyMap classification (1-µm map)	Nearby minerals (1-µm map)	HyMap classification (2-µm map)	Nearby minerals (2-µm map)
Kunak	Pegmatite	Pegmatites among Proterozoic shales and gneisses (marble,dolomite)	No data	Muscovite; garnet; cassiterite; orthite	Quartz; oligoclase	$Fe^{2+}Fe^{3+}$ Type2 (major)	$Fe^{2+}Fe^{3+}$ Type1, goethite (0.3 km north)	Illite* (major), muscovite (minor)	Calcite+montmorillonite, calcite and dolomite (0.3 km north)
Taghawlor deposit	Pegmatite	Pegmatites among Proterozoic shales in exocontact zone of Oligocene granites massif	Albitization	Spodumene; columbite-tantalite; cassiterite	Albite; microcline	$Fe^{2+}Fe^{3+}$ Type2 (major)		muscovite*, illite, chlorite or epidote, calcite mix	
Eskan	Poly-metallic vein	Oligocene granites	Silicification; limonitization	Limonite	Quartz	Not classified		muscovite* and calcite + muscovite/illite	
Waraz	Unk Cu	In the fracture zone which separates Lower Cretaceous ultrabasites from terrigenous-carbonate deposits of the same age	carbonatization	Malachite; azurite	No data	Not classified	Goethite (north), $Fe^{2+}Fe^{3+}$ Type2 and Fe^{3+} Type1 (south)	Not Classified*, calcite + montmorillonite (near), montmorillonite (near), calcite+musc/Illite, muscovite, calcite	
Awlamqul	Unk Hg	Lower Cretaceous limestones	Recrystallization; calcite alteration	Cinnabar; pyrite; hematite; realgar	Calcite; siderite; ankerite	Not classified (for a large area around prospect)	$Fe^{2+}Fe^{3+}$ Type2 (major)	Calcite (small groupings)	Calcite+musc/illite, muscovite, illite, dolomite, chlorite or epidote
Sewak	Unk Hg	Upper Jurassic - Lower Cretaceous limestones	Hematitization	Cinnabar; hematite	No data	Not classified (for a large area around prospect)	a few scattered pixels of goethite,Fe-hydroxide and Fe^{3+} Type1	Calcite (major)	Calcite + muscovite/illite

Name	Deposit type	Host lithology	Alteration	Mineralogy	Gangue	HyMap classification (1-µm map)	Nearby minerals (1-µm map)	HyMap classification (2-µm map)	Nearby minerals (2-µm map)
Solghoi	Unk Hg	Lower Cretaceous pebble conglom-erates	Recrystallization; bleaching; silicification; dickitization	Cinnabar; metacinnabarite; pyrite; hematite; chalcopyrite	Quartz; dickite; calcite; siderite; ankerite; barite	Goethite	Fe-hydroxide (bands of hematite north and south of prospect 0.3-0.5 km away)	Kaolinite + Muscovite/clay/calcite, Montmorillonite, muscovite (all mixed)	Calcite (0.75 km east and west of prospect)
Sheng	Vein Sn	Oligocene granites	Quartz alteration; silicification; limonitization	Pyrite; chalcopyrite; arsenopyrite; galena; limonite; malachite; azurite; cassiterite; scheelite	Quartz; muscovite; chlorite	Not classified	$Fe^{2+}Fe^{3+}$ Type2 with sacttered Fe^{3+} Type1	Muscovite (major)	Calcite + muscovite/illite, scattered pixels of kaolinite + muscovite/clay/ calcite
Chak	W skarn	A contact of Oligocene granites and Permian marbles forming a roof remnant	Skarn alteration	Scheelite	No data	Not classified	$Fe^{2+}Fe^{3+}$ Type2	Calcite + muscovite/illite	Muscovite with scattered pixels of calcite and kaolinite + muscovite/clay/ calcite
Charkh Tungsten	W unclassified	Oligocene granites and Proterozoic schists	Limonitization	No data	No data	Not classified and $Fe^{2+}Fe^{3+}$ Type2	Fe^{3+} Type1	Muscovite	Calcite + muscovite/illite, calcite and scattered chlorite or epidote
Salej	W unknown	Xenoliths of Proterozoic rocks within Oligocene granitoids stock	No data	No data	No data	Vegetation*, $Fe^{2+}Fe^{3+}$ Type2	small clusters of Fe^{3+} Type1,goethite and Fe-hydroxide)	Vegetation*, muscovite	Illite, scattered pixels of calcite and calcite + muscovite/illite
Charh II	W vein	No data	No data	No data	No data	$Fe^{2+}Fe^{3+}$ Type2* and not classified	Fe^{3+} Type1	Calcite + muscovite/illite and muscovite	Illite, calcite and scattered chlorite or epidote

Name	Deposit type	Host lithology	Alteration	Mineralogy	Gangue	HyMap classification (1-µm map)	Nearby minerals (1-µm map)	HyMap classification (2-µm map)	Nearby minerals (2-µm map)
Dariw-Sheng	W vein	Oligocene granites	Silicification; quartz alteration	Pyrite; chalcopyrite; fahlore; cassiterite; scheelite; malachite;	Quartz	Not classified	Fe^{3+} Type1,goethite, Fe-hydroxide, $Fe^{2+}Fe^{3+}$ Type2 (west) and vegetation	Calcite + montmorillonite, Calcite + muscovite/illite, muscovite and vegetation	
Nili	W vein	Oligocene granites	Greisen alteration; quartz alteration	Scheelite; wolframite; pyrite; chalcopyrite; bornite; cassiterite; bismuthinite; arsenopyrite	Quartz; muscovite	Not classified	$Fe^{2+}Fe^{3+}$ Type2 with scattered Fe^{3+} Type1	Muscovite and Illite	Calcite + montmorillonite and calcite + muscovite/illite with scattered calcite

* Mineral group at the exact pixel location of the known mineral occurrence.

There are three mercury prospects located within the Daykundi AOI. The Awlamqul prospect (lat 33°50'15"N, long 66°02'30"E) is located in the northwestern corner of the Daykundi AOI. The Early Cretaceous ore body occurs as mineralized zones within Lower Cretaceous limestones (Abdullah and others, 1977: Doebrich and others, 2006). The Sewak prospect (lat 34°14'26"N, long 66°52'44"E) occurs in Upper Jurassic – Lower Cretaceous limestones in the northeastern corner of the AOI. The mineralized area is in a zone that is approximately 70 × 150 m (Abdullah and others, 1977: Doebrich and others, 2006). The Solghoi prospect (lat 34°15'56"N, long 66°53'14"E) is located 2.8 km northeast of the Sewak prospect in the northeastern region of the AOI. The prospect occurs in a linear ore-bearing shatter zone within Lower Cretaceous pebble conglomerates that is approximately 300 × 500 m (Abdullah and others, 1977: Doebrich and others, 2006).

The Waraz prospect (lat 34°13'04"N, long 66°53'04"E) is the only named copper prospect in the Daykundi AOI. The prospect occurs in a fracture zone that separates Lower Cretaceous ultrabasites from terrigenous-carbonate deposits of the same age (Abdullah and others, 1977: Doebrich and others, 2006). In the fracture zone, the prospect occurs in 3 × 10 m lenses within a 300-m area (Abdullah and others, 1977: Doebrich and others, 2006).

5B.3.4 Data Limitations

Geographic registration between various datasets is not always possible because of differences in data collection methods and resolution. The geographic accuracy and quality of each dataset is limited by the original source. Significant efforts were made to ensure the geographic accuracy of the HyMap data. However, exact registration between previously published known mineral occurrences, fault traces, geologic units and structural boundaries in comparison to the HyMap data may not be ideal.

5B.4 Mineral Maps of the Daykundi Area of Interest

Analysis of the HyMap imaging spectrometer data of the Daykundi AOI using spectroscopic methods resulted in the identification of a wide variety of minerals exposed at the surface. Although the occurrence of certain minerals may suggest that mineralization processes may have once operated in the area, many of the minerals that were identified are also common rock-forming minerals or minerals that can be derived from the weathering of a wide variety of rock types. Consequently, knowledge about distribution patterns of the identified minerals and the geologic context in which they occur is essential for understanding the causes of mapped mineral occurrences and evaluating the possible potential for related mineral deposits.

Figures 5B–6*a* and 5B–7*a* depict, respectively, the distribution of the carbonates, phyllosilicates, sulfates, altered minerals, and other materials [2-micrometer (μm) map], and the iron-bearing minerals (1-μm map) for the Daykundi AOI. Both maps help identify different lithologies within the dataset, show regional trends, spatial relations of the different minerals, and may be used to improve the accuracy of future maps. Figures 5B–6*b* and 5B–7*b* show the same maps as figures 5B–6*a* and 5B–7*a*, with the addition of fault lines, geologic contacts, and known mineral occurrences.

Figures 5B–6*a* and 5B–6*b* show the distribution of the carbonates, phyllosilicates, sulfates, altered minerals, and other materials for the Daykundi AOI. The muscovite and illite classes dominate the AOI, and calcite mixed with clays/micas and the calcite classes also cover large parts of the area. Smaller contiguous areas of dolomite, chlorite or epidote, montmorillonite, serpentine and kaolinite + muscovite/clay/calcite are present throughout the region.

In the iron-bearing minerals map (figs. 5B–7*a* and 5B–7*b*), the Fe^{2+} Fe^{3+} Type 2, goethite classes, Fe^{3+} Type 1, and Fe-hydroxide classes dominate the AOI. Hematite and epidote are detected in smaller groupings in several areas. The Fe^{2+} Fe^{3+} Type 2 class composes a large percentage of the mapped pixels in the region. The Fe^{2+} Fe^{3+} Type 2 class is closely associated with the muscovite and illite classes in the 2-μm map (see fig. 5B–6*a*). The Fe^{2+} Fe^{3+} Type 2 class is usually detected within the pixels mapped as illite in the 2-μm map and less frequently in the muscovite class. Fe^{2+} Fe^{3+} Type 2 is detected in many units in the northeastern region but consistently occurs in Late Proterozoic (early part)

and Middle Proterozoic (early part) stratified rock units. In general, only the Precambrian stratified age rocks map as Fe^{2+} Fe^{3+} Type 2, and only minor amounts are detected in Paleozoic, Mesozoic, and Cenozoic age rocks. In the intrusive rocks, the Fe^{2+} Fe^{3+} Type 2 class is the dominant iron-bearing mineral present, but occurs in much smaller clusters throughout the area. Very few of the other iron-bearing minerals are detected in intrusive rocks. Most of the intrusive rocks are mapped as "not classified," and lack diagnostic spectral features in the 1-µm wavelength region.

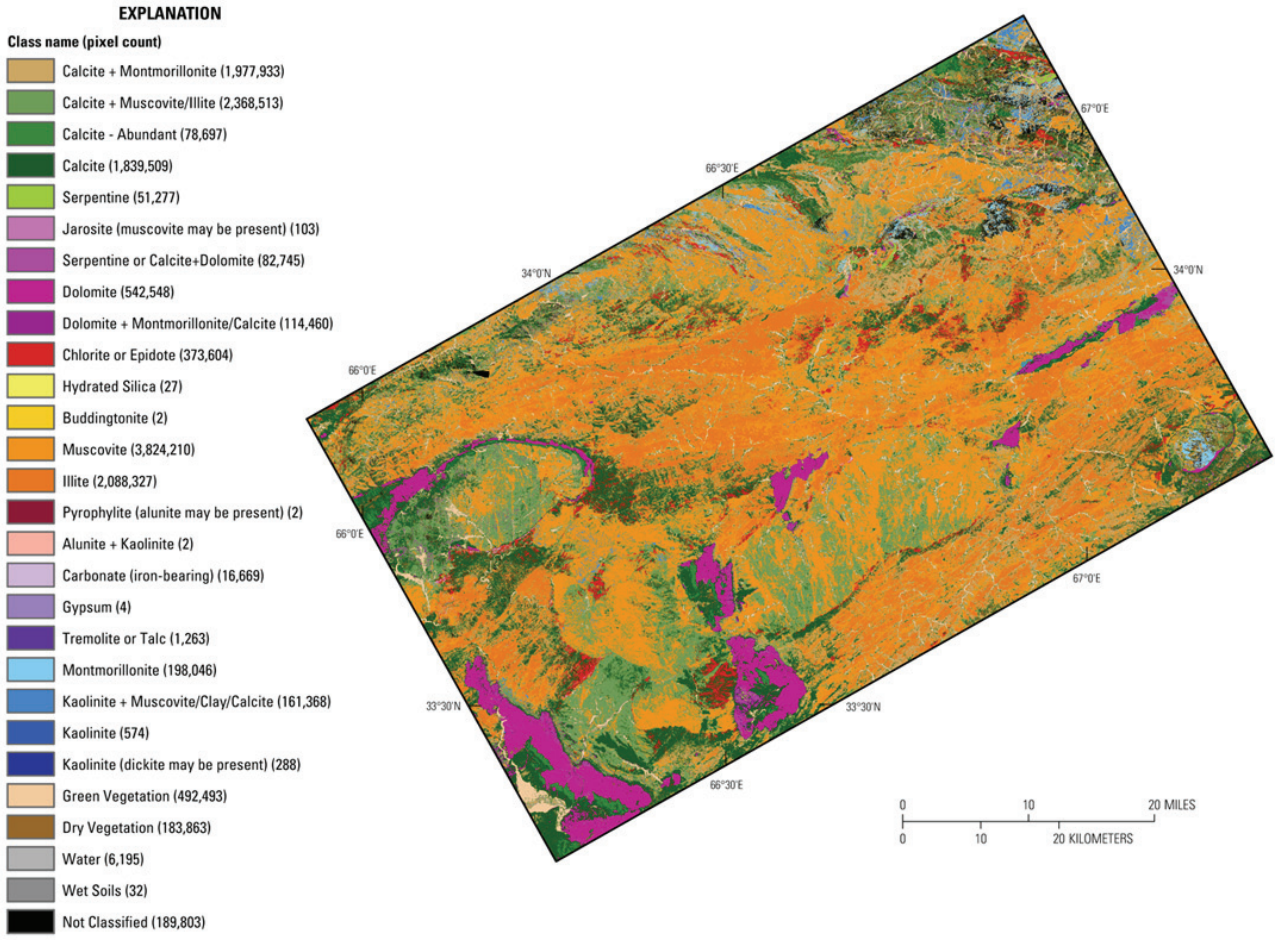

Figure 5B–6*a*. Map of carbonates, phyllosilicates, sulfates, altered minerals, and other materials derived from HyMap data in the Daykundi area of interest.

The Fe^{2+} Fe^{3+} type 1 class was found in only a small fraction of the total area of the Daykundi AOI, but those pixels are bound in small coherent clusters; these groupings are associated with the illite class in the 2-µm map (fig. 5B–6*a*). Two examples of where Fe^{2+} Fe^{3+} Type 1 is detected in clusters is near lat 33°47'30"N, long 66°22'52"E, and lat 33°56'25"N, long 66°33'53"E.

Because of the large number of classes represented and the subtleties of the distribution patterns represented in these image maps, it is instructive to display these results as a series of image maps, each depicting a selected group of minerals that are mineralogically related or commonly occur together in specific geologic environments (figs. 5B–8 through 5B–12). Figure 5B–8 shows the distribution of carbonate minerals in the Daykundi AOI, whereas figure 5B–9 shows where clay minerals and micas occur. The distribution of iron oxide and hydroxide minerals are displayed in figure 5B–10. Minerals commonly found in hydrothermally altered rocks are shown in figure 5B–11 and secondary minerals often associated with mineralized and/or weathered rocks are shown in figure 5B–12.

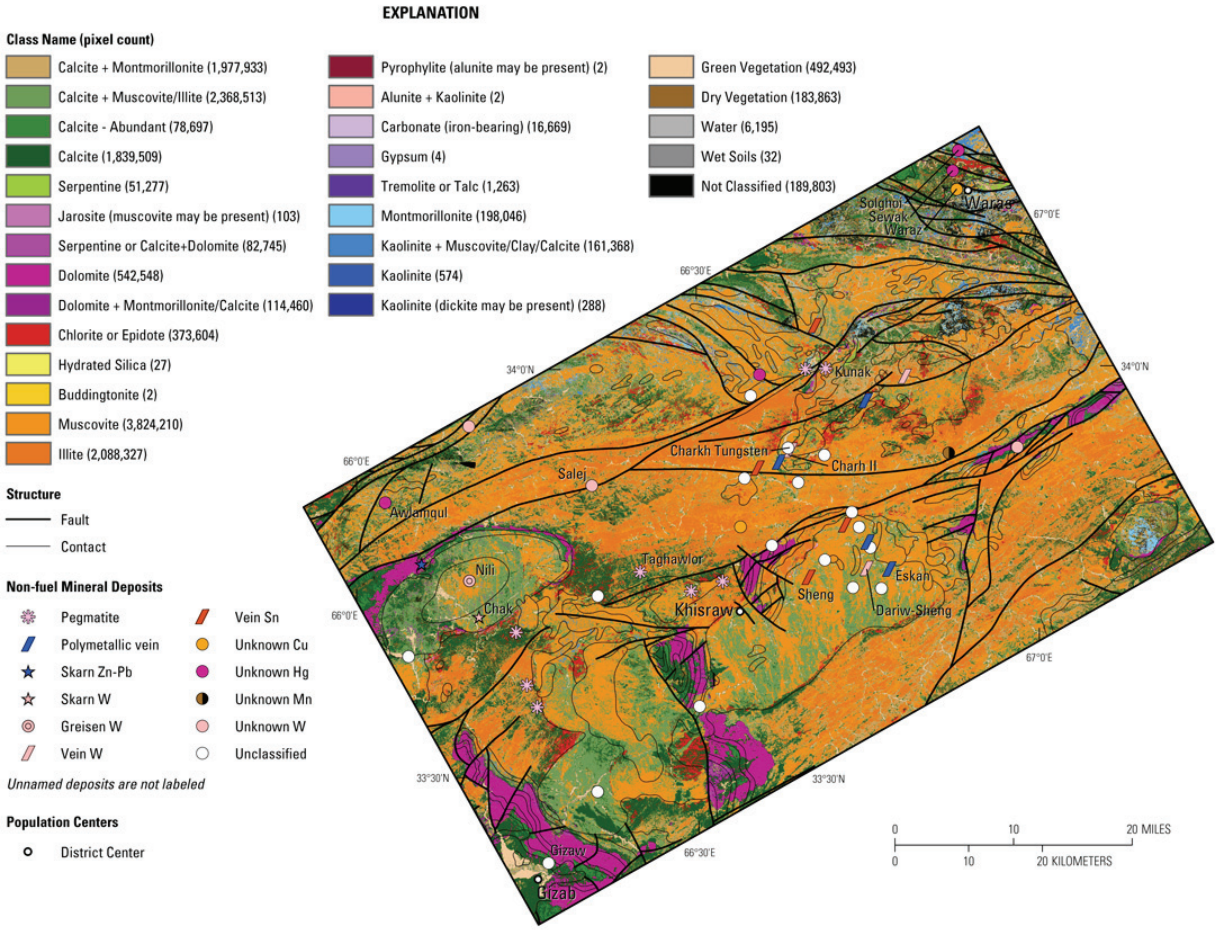

Figure 5B–6*b*. Map of carbonates, phyllosilicates, sulfates, altered minerals, and other materials derived from HyMap data with fault lines, geologic boundaries and known mineral occurrences (Doebrich and others, 2006; Abdullah and others, 1977; Peters and others, 2007) in the Daykundi area of interest.

5B.4.1 Carbonate Minerals

Carbonate minerals, either calcite + montmorillonite, calcite + muscovite/illite, dolomite or calcite were mapped over a large portion of the Daykundi AOI (fig. 5B–8). Although they are found in almost every rock unit, each individual class can be associated with different lithologic units. The calcite + montmorillonite class mainly occurs in Late Proterozoic (early part), Middle Proterozoic (early part), Middle Proterozoic (middle part) and Upper Aptian stage-Albian stratified rock units, with a smaller number of detections in the surrounding units. Contiguous areas of calcite + muscovite/illite are mapped within Middle Proterozoic (middle part) and Middle Proterozoic (early part) stratified rock units, and are clearly visible within the Oligocene intrusive age rocks (lat 33°44'26"N, long 66°13'38"E and lat 33°42'21"N, long 66°43'27"E).

The calcite class is present in almost every geologic unit. Calcite is commonly scattered throughout the units, but larger spatially coherent patterns can be seen in several areas near the mapped dolomite class minerals. Along the northern border of the AOI, large clusters of calcite form in Upper Aptian stage-Albian and Late Jurassic-Early Cretaceous stratified rocks. The dolomite class minerals dominate all stratified rock units between the ages of Early Permian to Carnian-Norian, with most of the pixels in these units mapped as dolomite or dolomite + montmorillonite/calcite. The carbonate (iron bearing) class is detected along the contact of stratified and igneous units near lat 33°41'02"N, long

66°11'40"E; lat 33°46'51"N, long 66°40'09"E, and near lat 33°31'37"N, long 66°17'56"E. It also is detected in clusters near the junction of three faults near lat 33°44'17"N, long 66°37'00"E.

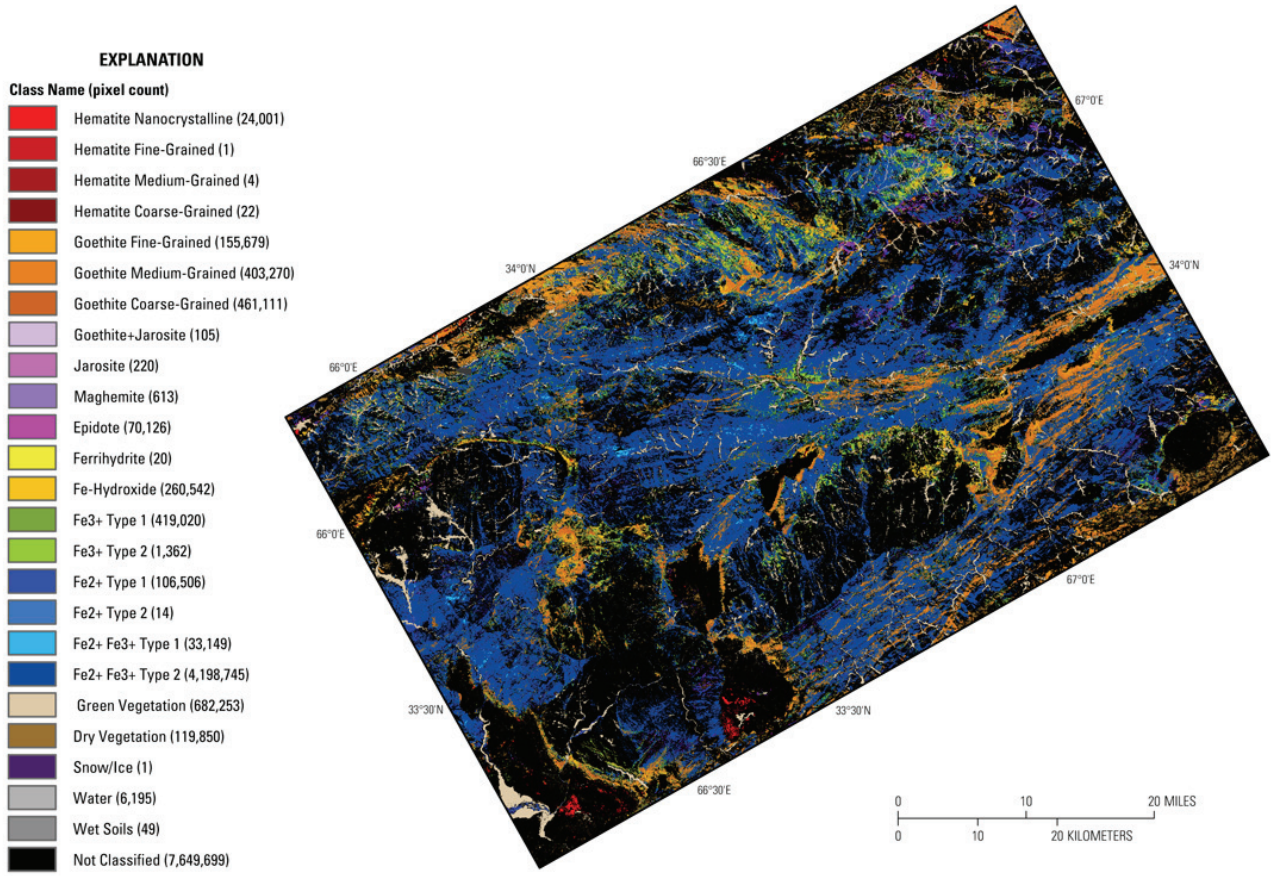

Figure 5B–7*a*. Map of iron-bearing minerals and other materials derived from HyMap data in the Daykundi area of interest.

5B.4.2 Clays and Micas

The calcite + montmorillonite and calcite + muscovite/illite mineral classes were removed from figure 5B–9 to improve clarity of the image because the calcite + clay/mica classes are detected over large regions within the AOI. The color of the illite class was changed to dark brown in this map to highlight its occurrence within the different lithologic units. The majority of the muscovite and illite classes map within Late Proterozoic (early part) and Middle Proterozoic (early part) stratified rock units and Proterozoic, Oligocene and Late Cretaceous-Paleocene intrusive age rocks. Although muscovite maps within most of the geologic units in the region, figure 5B–9 shows that the illite class is fairly constrained to the Late Proterozoic (early part) stratified rock unit. Early Permian through Carnian-Norian age stratified rocks contain little if any muscovite or illite. The muscovite mineral class dominates the Middle Proterozoic stratified rock unit and the Proterozoic, Oligocene and Late Cretaceous-Paleocene intrusive rocks. Muscovite does occur within Late Proterozoic (early part) age rocks, but is not as abundant as illite. The chlorite or epidote class is not mapped as large contiguous areas, but instead, as small groupings within a larger area.

Most of the dense groupings are in stratified rock units and occur near the contact with intrusive rocks. Two such areas are located at lat 33°32'46"N, long 66°18'42"E, and lat 33°41'39"N, long 66°13'33"E. Smaller groupings are present in almost all of the geologic units. Most of the kaolinite class minerals map in the northern and northeastern region of the Daykundi AOI. Large spatially consistent patterns of kaolinite occur in Late Jurassic-Early Cretaceous stratified rock units near lat 34°16'40"N,

long 66°54'11"E, and in one of the Oligocene intrusive units near lat 34°03'17"N, long 67°03'35"E. Kaolinite is mapped within the other Oligocene intrusive rocks, but within these units it is more dispersed. Kaolinite is detected in smaller groupings in Middle Proterozoic (early part) and Middle Proterozoic (middle part) stratified units and in Proterozoic intrusive rocks. Pixels matching the spectra of montmorillonite occur as small non-cohesive units throughout the northeastern region and are present in most of the rocks in this area of the AOI. The largest contiguous area of montmorillonite occurs in the Miocene intrusive rocks near lat 33°47'59"N, long 67°08'48"E. Here, montmorillonites are detected near the center of the intrusion with a dolomite/calcite contact zone around the edge of the intrusive body. In the 1-µm map (fig. 5B–7*a*) , goethite, Fe-hydroxide, Fe^{3+} Type 1, and a few pixels of epidote form an outer ring around the dolomite/calcite contact zone associated with muscovite in the 2-µm map (fig. 5B–6*a*). The combination of these minerals suggests that this area has the potential for mineralization.

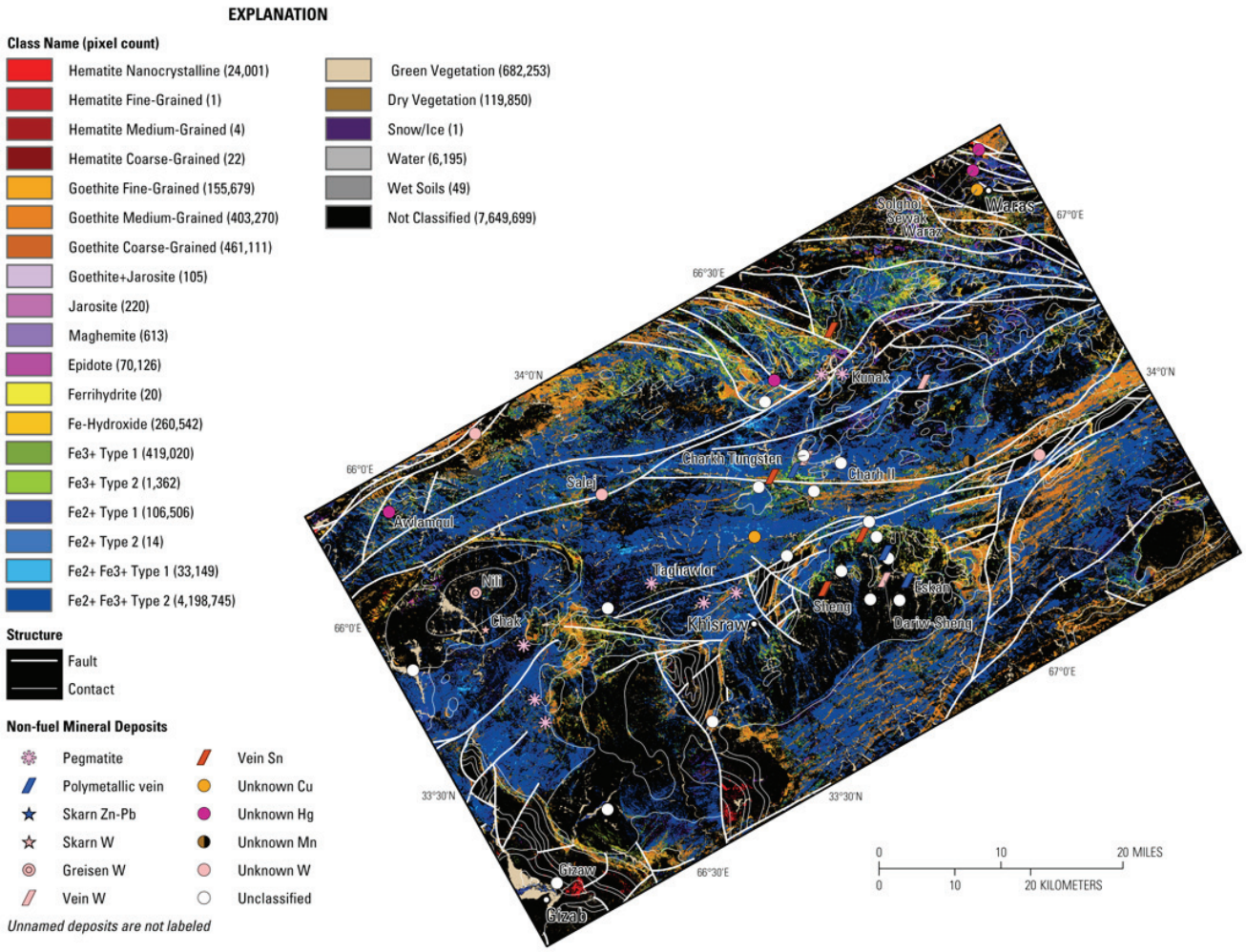

Figure 5B–7*b*. Map of iron-bearing minerals and other materials derived from HyMap data with fault lines, geologic boundaries, and known mineral occurrences (Doebrich and others, 2006; Abdullah and others, 1977; Peters and others, 2007) in the Daykundi area of interest.

5B.4.3 Iron Oxides and Hydroxides

The Daykundi AOI contains large areas of Fe-hydroxide and goethite (fig. 5B–10). Fe-hydroxide minerals are mapped along the edge of the AOI and are commonly associated with goethitic minerals in other parts of the Daykundi study area. Goethite is detected throughout the Daykundi AOI, but seems to occur in several geologically different areas. The largest contiguous areas of goethite group minerals occur adjacent to, or on the contact of, the dolomite units and in the units mapped as muscovite in the

2-µm map (fig. 5B–6*a*) in the southeastern region of the AOI (lat 33°47'59"N, long 67°08'48"E). In the northeastern corner, near lat 34°16'25"N, long 66°54'18"E goethite is associated with kaolinite. In intrusive rocks near lat 33°41'52"N, long 66°18'25"E, goethite (along with Fe-hydroxide and Fe^{3+} Type 1) is associated with kaolinite and muscovite in the 2-µm map (fig. 5B–6*a*). A large area of goethite is detected near lat 33°58'24"N, long 66°17'31"E and is mapped in rocks of different geologic ages. Two anomalous regions, near lat 33°29'20"N, long 66°31'29"E and lat 33°23'19"N, long 66°18'31"E, of hematite class minerals occur within the dolomite and calcite mineral classes (from the 2-µm map) in Permian and Triassic age stratified units (see King, Johnson, and others, 2011). Smaller clusters of hematitic minerals occur in Late Permian and Cretaceous age stratified rocks in the northwestern corner and north-central areas of the region.

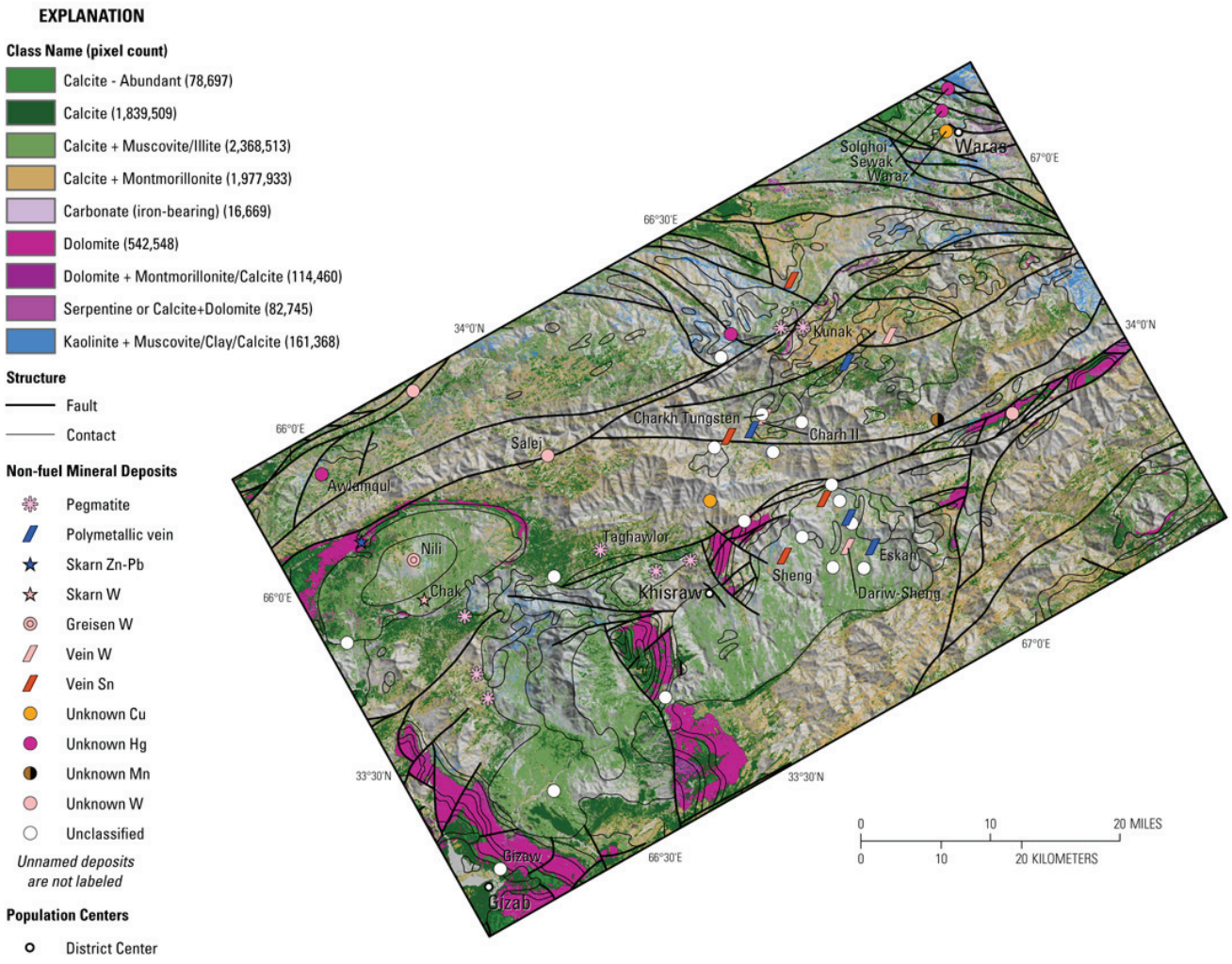

Figure 5B–8. Map of distribution of carbonate minerals derived from HyMap data in the Daykundi area of interest.

Most of the Fe-hydroxide and Fe^{3+} Type 1 classes are mapped within or near pixels of goethite. Many smaller groups of the Fe-hydroxide and Fe^{3+} Type 1 minerals map in different age rocks in the AOI. A large linear grouping of Fe-hydroxide and Fe^{3+} Type 1 minerals is present within Late-Permian-age stratified units in the northwestern part of the AOI. A large anomalous cluster of Fe-hydroxide, Fe^{3+} Type 1, and goethite pixels is detected in the Oligocene age intrusive rocks near lat 33°41'52"N, long 66°18'25"E (see King, Johnson, and others, 2011). Fe-hydroxide and Fe^{3+} Type 1 also map in large coherent clusters within Oligocene and Proterozoic age rocks near lat 34°01'55"N, long 67°04'26"E; and lat 34°03'05"N, long 66°39'31"E.

The epidote class minerals are detected as small dispersed groups and scattered pixels throughout the AOI, and spatially coincide with the chlorite or epidote class in the 2-µm map (fig. 5B–6*a*).

Most of the pixels in the maghemite class are scattered throughout the AOI, but small clusters detected within an area of Oligocene-age intrusive rocks near lat 34°01'02"N, long 66°53'01"E should be investigated more thoroughly. The rest of the mineral classes in the Fe-oxide and hydroxide map are detected as scattered or single pixel detections throughout the AOI, and show minimal association with rocks of specific ages or types.

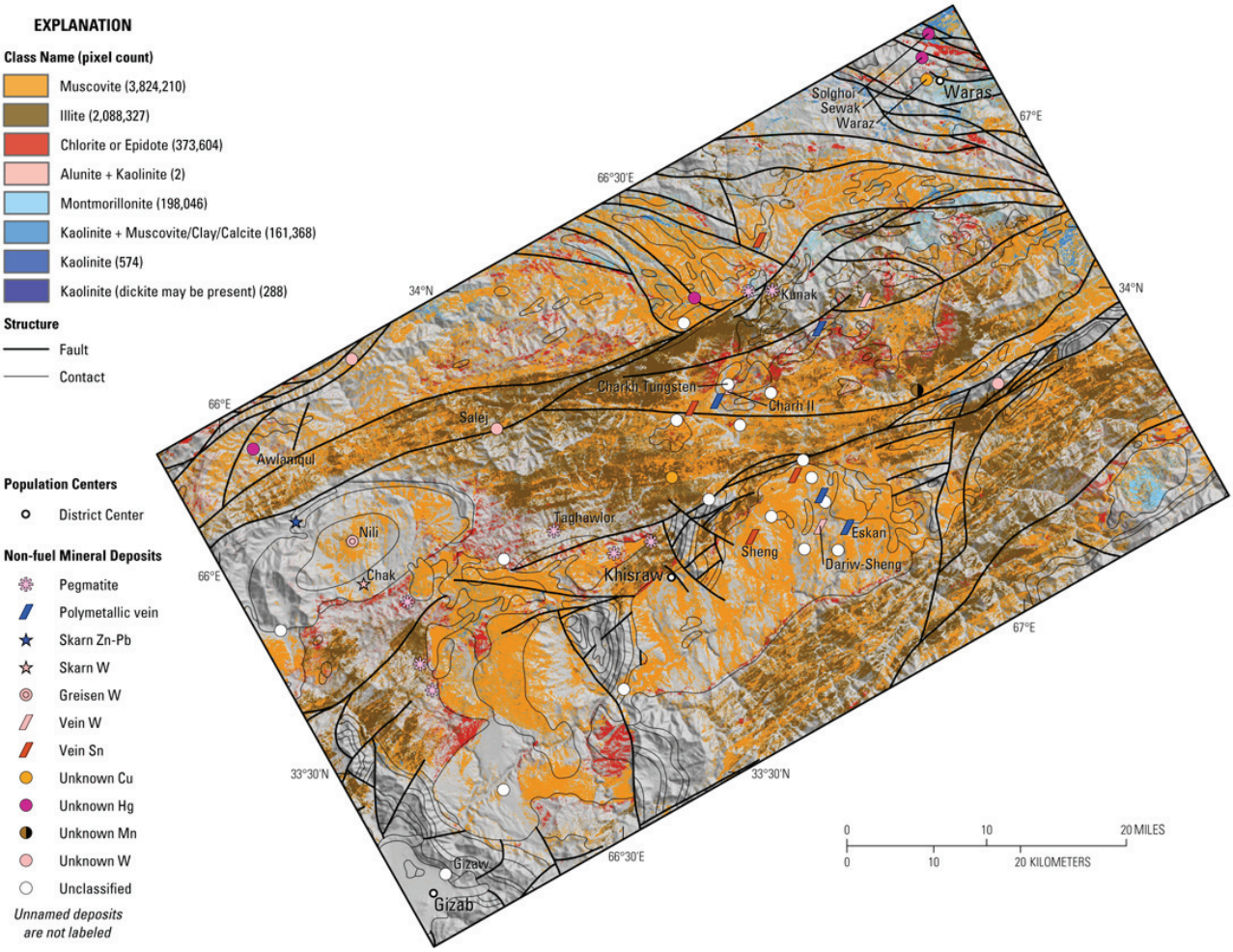

Figure 5B–9. Map of distribution of clay and mica minerals derived from HyMap data in the Daykundi area of interest.

5B.4.4 Common Alteration Minerals

Most of the minerals in this group are commonly present in hydrothermally altered rocks associated with epithermal mineral deposits (fig. 5B–11). Consequently, the locations of distinct clusters are of great interest in terms of potential mineral deposits. The chlorite or epidote class minerals are detected throughout the AOI and are associated with rocks of several different ages. In the southwestern region, chlorite or epidote group minerals are mapped in stratified units that are in contact with intrusive rocks (lat 33°32'46"N, long 66°18'42"E, and lat 33°41'39"N, long 66°13'33"E). Smaller groupings are mapped in most the geologic units. Kaolinite group minerals are detected in several units of stratified and intrusive rocks. Large spatially consistent patterns of kaolinite occur in Late Jurassic-Early Cretaceous stratified rock units near lat 34°16'40"N, long 66°54'11"E and in one of the Oligocene intrusive units near lat 34°03'17"N, long 67°03'35"E. The carbonate (iron bearing) class is detected along the contact of stratified and igneous units near lat 33°41'02"N, long 66°11'40"E; lat 33°46'51"N, long

66°40'09"E, and near lat 33°31'37"N, long 66°17'56"E, and in clusters near the junction of three faults at lat 33°44'17"N, long 66°37'00"E.

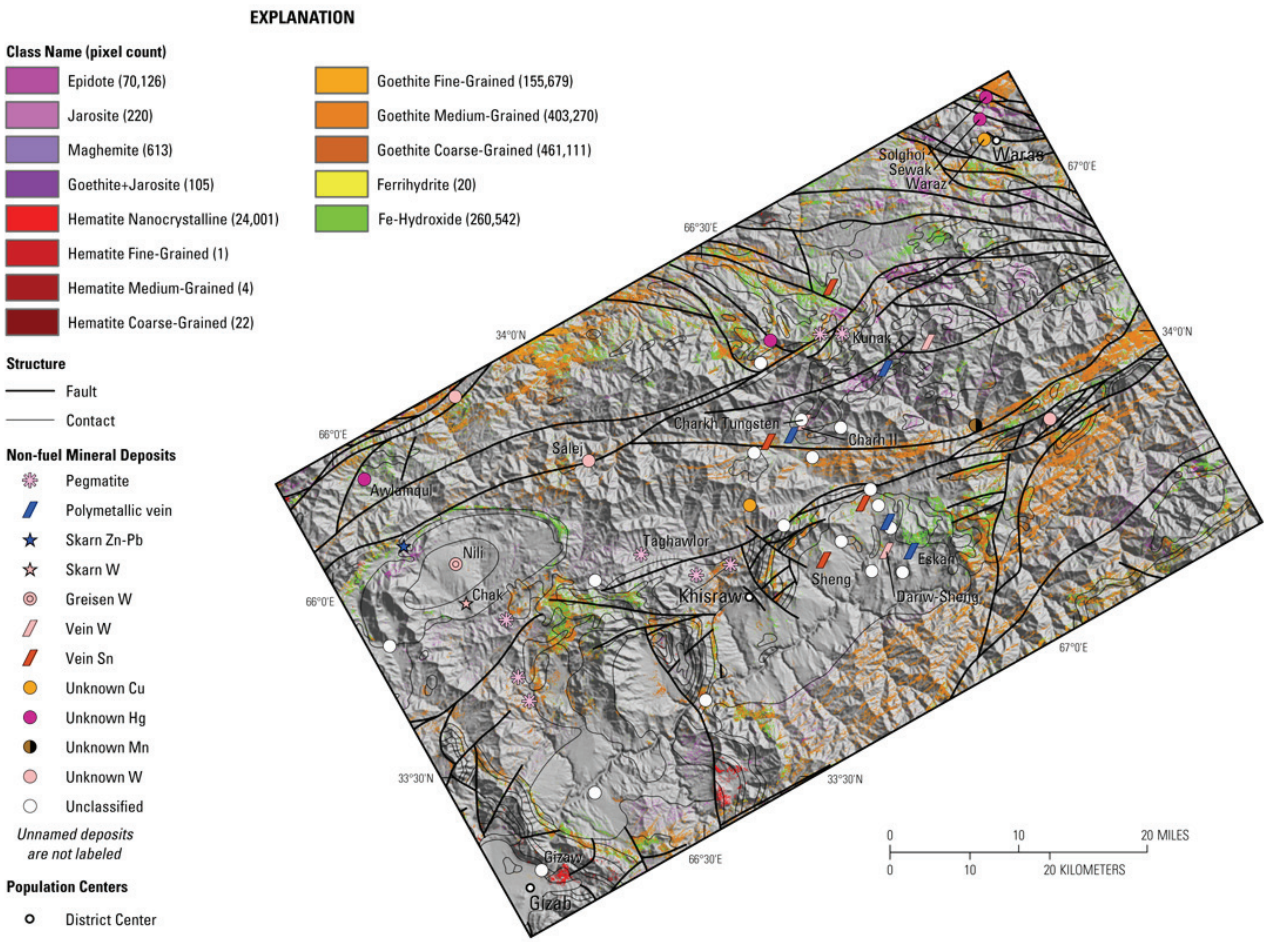

Figure 5B–10. Map of distribution of iron oxide and hydroxide derived from HyMap data in the Daykundi area of interest.

5B.4.5 Common Secondary Minerals

The only mineral class highlighted in figure 5B–12 is the chlorite or epidote mineral class, which is detected in many areas throughout the AOI. In several areas, the chlorite or epidote mineral class is detected along the contact between intrusive and stratified units that contains greenstone or greenschist rocks (lat 34°14'56"N, long 66°54'36"E and lat 34°04'06"N, long 66°56'05"E). The serpentine mineral class is detected almost exclusively within the Early Cretaceous intrusive rocks in the northeastern region of the AOI. The two largest occurrences are mapped near lat 34°13'13"N, long 66°56'11"E and lat 34°01'13"N, long 66°43'57"E in rocks described as being composed of dunite, peridotite, and serpentinite by Doebrich and others (2006) and Abdullah and Chmyriov (1977). The HyMap mapping results identified minerals that are consistent with this lithology. The "serpentine or calcite + dolomite" class is mapped within several different geologic units, and in most locations, along the edge of the dolomite class.

Tremolite or talc detections mostly occur in the northeastern region in many different geologic units. Most groupings are very small and scattered throughout the area. The only significantly large grouping occurs near lat 34°03'56"N, long 66°45'30"E.

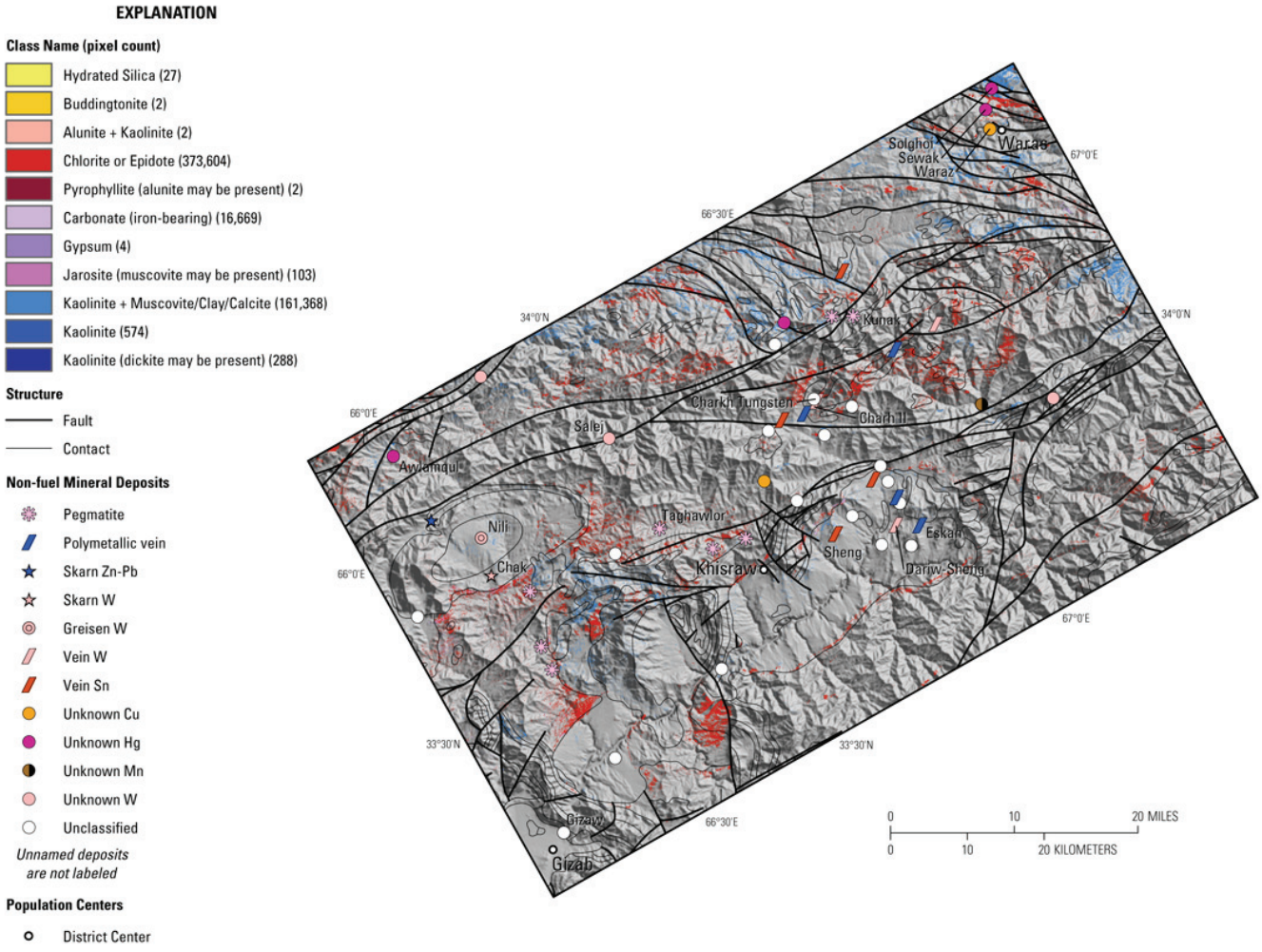

Figure 5B–11. Map of distribution of common alteration minerals derived from HyMap data in the Daykundi area of interest.

5B.4.6 Mineral Maps and Known Mineral Occurrences

There are 49 known mineral occurrences listed in table 5B–1, most of which are either unnamed or listed as unknown or unclassified deposit types. Usually these mineral occurrences are very small or little information is known about them. In table 5B–2, only the larger known mineral occurrences that have names have been included. The table includes HyMap classifications of the 1- and 2-µm maps as they relate to the immediate area around each known mineral resource, as well as a list of any nearby mineral groups that could be associated with the known mineral occurrences.

Most of the large known mineral occurrences are classified into one of the following three types of prospects: pegmatites, unknown mercury, and tungsten. The Kunak prospect (lat 34°00'00" N, long 66°41'23" E) and Taghawlor (lat 33°46'07" N, long 66°24'58"E) deposit are the two large pegmatite prospects in the Daykundi AOI. The area around the Kunak prospect is dominated by illite and muscovite, with relatively few other detections in the 2-µm map (fig. 5B–6*a*), and Fe^{2+} Fe^{3+} Type 2 in the 1-µm map (fig. 5B–7*a*). Muscovite is listed by Doebrich and others (2006) and Abdullah and Chmyriov (1977) as one of the minerals associated with the Kunak prospect, and this is consistent with the 2-µm mapping results. The Taghawlor deposit is located within a group of pixels that include muscovite, illite, calcite, with a few pixels of chlorite or epidote in the 2-µm map, and Fe^{2+} Fe^{3+} Type 2 in the 1-µm map. Most of the minerals associated with the Taghawlor deposit as described by Doebrich

and others (2006) and Abdullah and others (1977) lack diagnostic absorption bands in the 0.43- to 2.48-µm region, and therefore, the HyMap detections are consistent with the host rock for the area.

The Awlamqul (lat 33°50'15"N, long 66°02'30"E), Sewak (lat 34°14'26"N, long 66°52'44"E), and Solghoi (lat 34°15'56"N, long 66°53'14"E) prospects are all mercury deposit types. The Awlamqul and Sewak prospects are both associated with areas of calcite in the 2-µm map and areas that mapped as "not classified" in the 1-µm map (fig. 5B–7*a*). The host lithologies for these two prospects are listed as limestones by Doebrich and others (2006) and Abdullah and Chmyriov (1977), which agrees with the mapping results for both areas. The Solghoi prospect is located on the border of Upper Aptian stage-Albian and Late Jurassic-Early Cretaceous stratified rock units. Gangue materials are listed as quartz, dickite, calcite, siderite, ankerite, and barite (Doebrich and others, 2006; Abdullah and Chmyriov,1977). HyMap detections for the area near the Solghoi prospect include kaolinite + muscovite/clay/calcite, montmorillonite, and muscovite, with a majority of pixels in the immediate vicinity of the location of the prospect being kaolinite + muscovite/clay/calcite. In the 1-µm map, the prospect is located on the border of pixels matching the spectra of goethite/Fe-hydroxide and a region mapped as not classified. The 2-µm map detections of kaolinite + muscovite/clay/calcite near the known prospect location is consistent with the listed gangue material of calcite (Doebrich and others, 2006; Abdullah and Chmyriov, 1977).

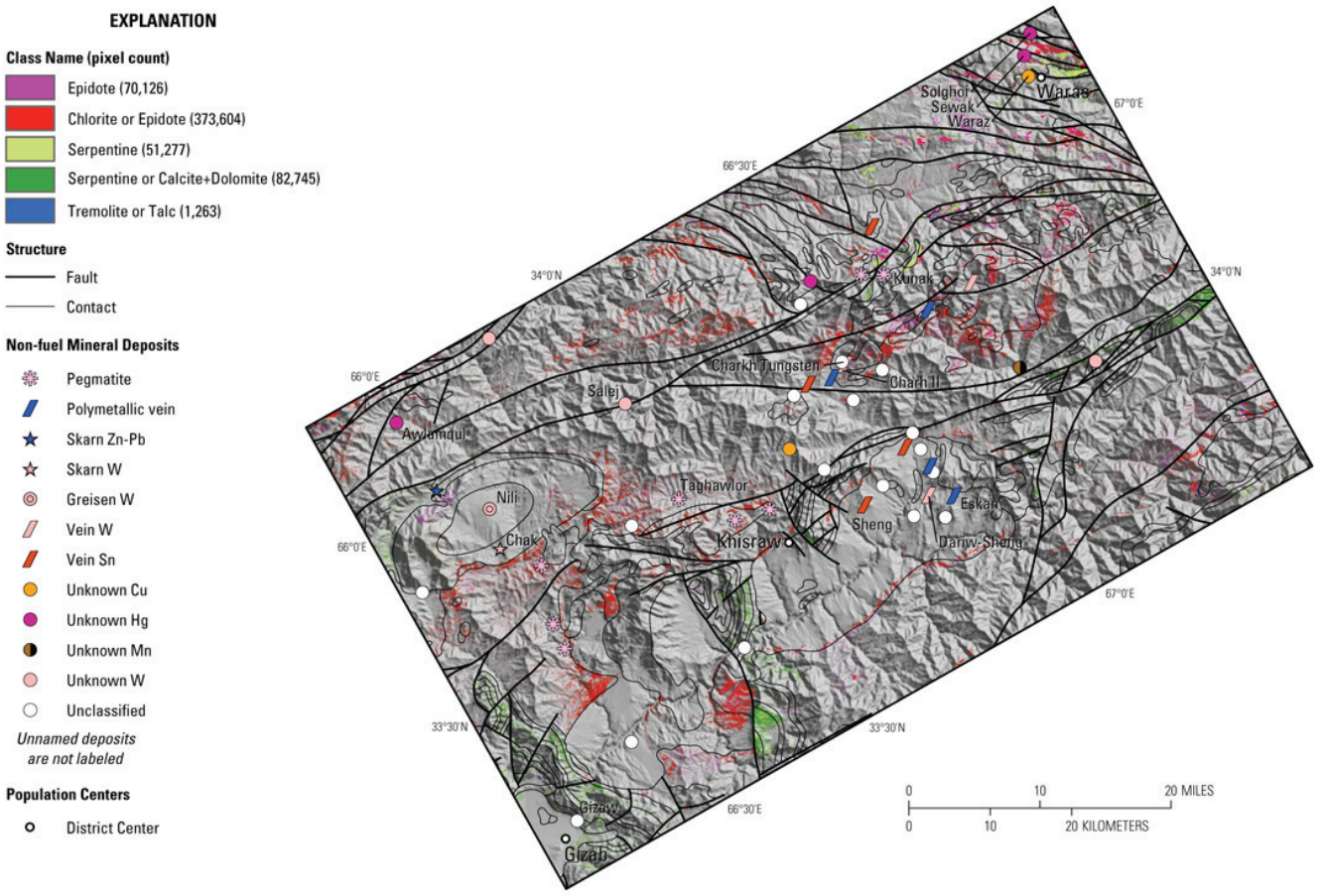

Figure 5B–12. Map of distribution of common secondary minerals derived from HyMap data in the Daykundi area of interest.

The Daykundi AOI has six known tungsten prospects with names. The Charkh (lat 33°54'10"N, long 66°38'00"E), Nili (lat 33°44'29"E, long 66°09'55"E), Chak (lat 33°41'40"N, long 66°10'40"E) and Dariw-Sheng (lat 33°45'17"N, long 66°44'51"E) prospects are all located in Oligocene age granodiorites and granites (Abdullah and others, 1977; Doebrich and others, 2006). The Salej (lat 33°51'30"N, long

66°20'30"E) and Charh II (lat 33°54'11"N, long 66°38'00"E) tungsten prospects are located within Late Proterozoic (early part) stratified rock units. The Salej prospect is mapped within the vegetation group surrounded by pixels of muscovite, illite, calcite + muscovite/illite and calcite in the 2-μm map (fig. 5B–6*a*). In the 1-μm map (fig. 5B–7*a*), the Salej prospect is mapped within the vegetation group surrounded by pixels of Fe^{2+} Fe^{3+} Type 2, goethite classes, Fe^{3+} Type 1, and Fe-hydroxide. The Charh II prospect is located within a region dominated by muscovite, with occasional detections of illite, calcite + muscovite/illite, and calcite in the 2-μm map, and Fe^{2+} Fe^{3+} Type 2 in the 1-μm map. Little is known about either prospect, but the location of the Charh II prospect is within 0.15 km of an Oligocene-age intrusive body, so it may be associated with intrusive rocks. The rest of the tungsten prospects are located within an area of muscovite group minerals (muscovite or calcite + muscovite/illite) in the 2-μm map, that are consistent with the host granodioritic/granitic rocks. Most spectra of rocks within the Oligocene-age intrusive body lack diagnostic features in the 1-μm region, and as a result, most of the area around these prospects is in the "not classified" category in the iron-bearing materials map.

The Sheng prospect is a tin prospect located near lat 33°44'39"N, long 66°39'45"E, and the Eskan prospect is a polymetallic vein prospect type located near lat 33°45'00"N, long 66°47'00"E. The Sheng prospect and many of the other much smaller tin prospects, as well as the Eskan polymetallic vein prospect, are located in Oligocene-age intrusive granodiorites and granites that correlate to the muscovites class materials in the 2-μm map (fig. 5B–6*a*) and are not classified group in the 1-μm map (fig. 5B–7*a*).

5B.5 Summary

The HyMap data for the Daykundi area shows several locations, based on the presence of specific minerals or groups of minerals, that suggest the need for additional field sampling, geophysical and geochemical characterization. The HyMap data were used to identify and delineate the different lithologic units and their spatial relations in the Daykundi AOI.

The calcite, calcite + clays/micas, muscovite and illite mineral classes dominate the AOI. Large contiguous areas of dolomite, chlorite or epidote, montmorillonite, serpentine and kaolinite + muscovite/clay/calcite are mapped throughout the region. Muscovites and illites are widespread in the AOI, and the illite class seems to be constrained to the Late Proterozoic (early stage) age rocks. In most of the intrusive rocks, with the exception of Early Cretaceous age rocks, illite is absent and muscovite dominates the units. The serpentine mineral class is detected almost exclusively within the Early Cretaceous age intrusive rocks in the northeastern region with two of the larger concentration located near lat 34°13'13"N, long 66°56'11"E, and lat 34°01'13"N, long 66°43'57"E. Near lat 34°01'07"N, long 66°44'05"E; lat 34°01'03"N, long 66°41'07"E; and lat 34°14'34"N, long 66°55'38"E, the serpentine class minerals are associated with the chlorite or epidote class minerals. One of the most interesting features in the Daykundi AOI is a well-defined, rounded Miocene-age intrusive body located near lat 33°47'59"N, long 67°09'33"E. The central zone of the intrusive body maps as montmorillonite, with scattered pixels of calcite + montmorillonite and muscovite toward the margins. At the contact of the Miocene age intrusive rocks and the Late Proterozoic (early part) age stratified rocks is a contact zone of dolomite and calcite. In the 1-μm map, goethite, Fe-hydroxide, Fe^{3+} Type 1, and a few pixels of epidote form a ring around the outer edge of the dolomite/calcite contact zone, and are associated with muscovites in the 2-μm map. Iron-bearing materials are not detected within the Miocene intrusive unit. The presence of these material groups within and around the Miocene intrusive body is suggestive of an area of potential mineralization worthy of additional field work and characterization.

The dolomite, dolomite + montmorillonite/calcite and calcite classes are detected in Early Permian to Carnian-Norian stratified rocks . The dolomites are visible in the southwestern part of the AOI and in a narrow linear band in the west-central region. As mentioned above, the dolomite mineral class also forms at the contact zone between the Miocene intrusive rocks and Late Proterozoic (early part) age stratified rocks in the southeastern corner of the AOI. Iron carbonates commonly map along the

contact between the stratified rock units and intrusive rocks near lat 33°41'02"N, long 66°11'40"E; lat 33°46'51"N, long 66°40'09"E; and lat 33°31'37"N, long 66°17'56"E.

In the iron-bearing map (fig. 5B–7*a* and fig. 5B–7*b*), the Fe^{2+} Fe^{3+} Type 2, goethite classes, Fe^{3+} Type 1, and Fe-hydroxide classes are the dominant minerals with lesser amounts of hematite and epidote. The Fe^{2+} Fe^{3+} Type 2 class is closely associated with the muscovite and illite classes detected in the 2-µm map. In general, Fe^{2+} Fe^{3+} Type 2 class minerals are detected extensively in the Precambrian stratified age rocks, with minor occurrences in Paleozoic, Mesozoic and Cenozoic age rocks. In the intrusive rocks, there is a lack of detected iron-bearing materials, the most abundant of which is the Fe^{2+} Fe^{3+} Type 2 class. Most of the area within the intrusive rocks is mapped as "not classified." The largest contiguous areas of goethite seem to occur adjacent to, or in contact with, the dolomite units in the 2-µm map or in the units mapped as muscovite in the southeastern region of the AOI. In other areas, goethite is associated with kaolinites (lat 34°04'22"N, long 66°32'0947"E, and lat 33°39'24"N, 66°19'07"E). Most of the Fe-hydroxide and Fe^{3+} Type 1 classes are associated with goethite and are often detected as mixed pixels with goethite or along the contact with goethite throughout the region. The epidote class maps as small dispersed groupings and scattered pixels throughout the AOI. The Fe^{2+} Fe^{3+} Type 1 class is mapped within a small area of the Daykundi AOI, but these pixels are bound in coherent groupings. The Fe^{2+} Fe^{3+} Type 1 groupings are associated with the illite class in the 2-µm map. Two anomalous regions of the hematite class minerals (lat 33°29'20"N, long 66°31'29"E, and lat 33°23'19"N, 66°18'31"E) occur within the dolomite and calcite classes in Permian and Triassic age stratified units (see King, Johnson, and others, 2011).

Although there are many prospects in the Daykundi area, according to Abdullah and others (1977), many of these are small skarns or small prospects that are most likely sub-pixel occurrences. Many of the associated minerals that occur within these prospects also lack diagnostic absorption features in the 0.43- to 2.48-µm region. As a result, most of the HyMap classes do not correlate well with any unnamed, unknown, or unclassified mineral occurrence.

Most of the larger known mineral occurrences are pegmatite, mercury, or tungsten type prospects. The area around the Kunak pegmatite prospect is mapped as muscovite and illite in the 2-µm map and Fe^{2+} Fe^{3+} Type 2 in the 1-µm map. Muscovite is consistent with the mineralogy of the prospect as described by Abdullah and others (1977) and Doebrich and others (2006). The Taghawlor deposit is mapped within a group of pixels that include muscovite, illite, and calcite, with a few pixels of chlorite or epidote in the 2-µm map, and Fe^{2+} Fe^{3+} Type 2 in the 1-µm map, and is more consistent with the host rocks then anything described by Abdullah and others (1977) and Doebrich and others (2006) in relation to the known mineral occurrence.

The Awlamqul, Sewak, and Solghoi prospects are all mercury prospects. The Awlamqul and Sewak prospects are both associated with limestone, and this is consistent with the HyMap detections of calcite in the area in the 2-µm map and areas that are mapped as "not classified" in the 1-µm map. The 2-µm map detections of kaolinite + muscovite/clay/calcite near the location of the Solghoi known mineral occurrence is consistent with the listed gangue material of calcite (Doebrich and others, 2006; and Abdullah and Chmyriov, 1977).

The Sheng prospect and many of the other much smaller tin prospects, as well as the Eskan polymetallic vein prospect, are located in Oligocene-age intrusive granodiorites and granites that correlate to the muscovites class materials in the 2-µm map and the "not classified" group in the 1-µm map. The HyMap detections are consistent with minerals typically associated with granitic rocks.

Muscovite or calcite + muscovite/illite are detected at the Charkh, Nili, Chak, and Dariw-Sheng tungsten prospects, and all four are located in Oligocene age granodiorites or granites. Again, muscovite is a common mineral in granitic rocks, and the result is expected in the HyMap classifications. Little historical information is available for the Char II and Salej tungsten prospects. Illite, calcite + muscovite/illite and calcite are detected at the Char II prospect in the 2-µm map, and Fe^{2+} Fe^{3+} Type 2 are detected in the 1-µm map. At the Salej prospect, muscovite, illite, calcite + muscovite/illite, and

calcite are detected in the 2-μm map, and Fe^{2+} Fe^{3+} Type 2, goethite classes, Fe^{3+} Type 1, and Fe-hydroxide are detected in the 1-μm map.

5B.6 References Cited

Abdullah, Sh., and Chmyriov, V.M., eds., 1977, Map of mineral resources of Afghanistan: Kabul, Afghanistan, Ministry of Mines and Industries of the Democratic Republic of Afghanistan, Department of Geological and Mineral Survey, V/O "Technoexport" USSR, scale 1:500,000.

Abdullah, Sh., Chmyriov, V.M., Stazhilo-Alekseev, K.F., Dronov, V.I., Gannan, P.J., Rossovskiy, L.N., Kafarskiy, A.Kh., and Malyarov, E.P., 1977, Mineral resources of Afghanistan (2d ed.): Kabul, Afghanistan, Republic of Afghanistan Geological and Mineral Survey, 419 p.

Cocks, T., Jenssen, R., Stewart, A., Wilson, I., and Shields, T., 1998, The HyMap airborne hyperspectral sensor—The system, calibration and performance, *in* Schaepman, M., Schlapfer, D., and Itten, K.I., eds., Proceedings of the 1st EARSeL Workshop on Imaging Spectroscopy, 6–8 October 1998, Zurich: Paris, European Association of Remote Sensing Laboratories, p. 37–43.

Davis, P.A., 2007, Landsat ETM+ false-color image mosaics of Afghanistan: U.S. Geological Survey Open-File Report 2007–1029, 22 p. (Also available at *http://pubs.usgs.gov/of/2007/1029/*.)

Doebrich, J.L., and Wahl, R.R., comps., with contributions by Doebrich, J.L., Wahl, R.R., Ludington, S.D., Chirico, P.G., Wandrey, C.J., Bohannon, R.G., Orris, G.J., Bliss, J.D., and ____, 2006, Geologic and mineral resource map of Afghanistan: U.S. Geological Survey Open File Report 2006–1038, scale 1:850,000, available at *http://pubs.usgs.gov/of/2006/1038/*.

Hoefen, T.M., Kokaly, R.F., and King, T.V.V., 2010, Calibration of HyMap data covering the country of Afghanistan, *in* Proceedings of the 15th Australasian Remote Sensing and Photogrammetry Conference, Alice Springs, Australia, September 12–17, 2010, p. 409, available at *http://dl.dropbox.com/u/81114/15ARSPC-Proceedings.zip/*.

King, T.V.V., Johnson, M.R., Hoefen, T.M., Kokaly, R.F., and Livo, K.E., 2011, Mapping potential mineral resource anomalies using HyMap data, *in* King, T.V.V., Johnson, M.R., Hubbard, B.E., and Drenth, B.J., eds, Identification of mineral resources in Afghanistan—Detecting and mapping resource anomalies in prioritized areas using geophysical and remote sensing (ASTER and HyMap) data in Afghanistan: U.S. Geological Survey Open-File Report 2011–1229, available at *http://pubs.usgs.gov/of/2011/1229/*.

King, T.V.V., Kokaly, R.F., Hoefen, T.M., Dudek, K. and Livo, K.E., 2011, Surface materials map of Afghanistan—Iron-bearing minerals and other materials: U.S. Geological Survey Scientific Investigations Map 3152–B.

King, T.V.V., Kokaly, R.F., Hoefen, T.M., and Knepper, D.H., 2010, Resource mapping in Afghanistan using HyMap data, *in* Proceedings of the 15th Australasian Remote Sensing and Photogrammetry Conference, Alice Springs, Australia, September 12–17, 2010, p. 500, available at *http://dl.dropbox.com/u/81114/15ARSPC-Proceedings.zip/*.

Kokaly, Ray, 2011, PRISM—Processing routines in IDL for spectroscopic measurements: U.S. Geological Survey Open-File Report 2011–1155, available at *http://pubs.usgs.gov/of/2011/1155/*.

Kokaly, R.F., King, T.V.V., and Livo, K.E., 2008, Airborne hyperspectral survey of Afghanistan 2007—Flight line planning and HyMap data collection: U.S. Geological Survey Open-File Report 2008–1235, 14 p.

Kokaly, R.F., King, T.V.V., Hoefen, T.M., Dudek, K. and Livo, K.E., 2011, Surface materials map of Afghanistan—Carbonates, phyllosilicates, sulfates, altered minerals, and other materials: U.S. Geological Survey Scientific Investigations Map 3152–A.

Peters, S.G., Ludington, S.D., Orris, G.J., Sutphin, D.M., Bliss, J.D., and Rytuba, J.J., eds., and the U.S. Geological Survey-Afghanistan Ministry of Mines Joint Mineral Resource Assessment Team, 2007, Preliminary non-fuel mineral resource assessment of Afghanistan: U.S. Geological Survey Open-File Report 2007–1214, 810 p., 1 CD–ROM. (Also available at *http://pubs.usgs.gov/of/2007/1214/*.)